Ocean Modelling 186 (2023) 102261

Contents lists available at ScienceDirect

Ocean Modelling

journal homepage: www.elsevier.com/locate/ocemod

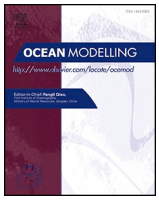

Impact of vertical resolution on representing baroclinic modes and water mass distribution in the North Atlantic☆

Xiaobiao Xu *, Eric P. Chassignet, Alan J. Wallcraft

Center for Ocean-Atmospheric Prediction Studies, Florida State University, United States

ARTICLE INFO

Keywords:
Vertical resolution
Baroclinic modes
Water masses
AMOC
North Atlantic
OGCMs

ABSTRACT

In contrast to the large volume of studies on the impact of horizontal resolution in oceanic general circulation models (OGCMs), the impact of vertical resolution has been largely overlooked and there is no consensus on how one should construct the vertical grid to represent the vertical structure of the baroclinic modes as well as the distribution of distinct water masses throughout the global ocean. In this paper, we document the importance of vertical resolution in the representations of vertical modes and water masses in the North Atlantic and show i) that vertical resolution is unlikely to undermine the resolution capability of the horizontal grid in representing the vertical modes and a 32-layer isopycnal configuration is adequate to represent the first five baroclinic modes in mid-latitudes and ii) that vertical resolution should focus on representing water masses. A coarse vertical resolution (16-layer) simulation exhibits virtually no transport in the dense overflow water which leads to a weaker and significantly shallower Atlantic meridional overturning circulation (AMOC) despite resolving the first baroclinic mode throughout the domain, whereas there are overall very small differences in the subtropical and subpolar North Atlantic circulation in the simulations with finer vertical resolution (24 to 96 layers). We argue that accurately representing the water masses is more important than representing the baroclinic modes for an OGCM in modeling the low-frequency large-scale circulation.

1. Introduction

Oceanic general circulation models (OGCMs), with the underlying algorithmic formulation principles first proposed by Bryan (1969) in the 1960s (McWilliams 1996), have become an essential supplement to the more traditional methodologies in physical oceanography, i.e., theory and observations, and have a wide range of applications (e.g., Le Sommer et al., 2018). They are used to test hypotheses for mechanisms underlying oceanic observations in idealized or realistic configurations, to study the Earth's climate variability on seasonal to decadal time scales and to assess future scenarios from changes in anthropogenic forcing when coupled with the ice, atmosphere, and land components of the climate system, and to generate short-term ocean forecasts or long-term reanalysis when integrated in a data-assimilation framework. These applications offer valuable insights on various aspects of the ocean circulation and its role in the Earth's climate.

Due to finite computational resources and discretized equations of motion, not all processes can be accurately represented in OGCMs and some of them need to be parameterized. Thus, the OGCM's horizontal and vertical grid spacing is and will remain the fundamental parameters for any configuration. For example, the horizontal grid spacing determines to what extent an ocean model can resolve mesoscale eddies, which represents close to 80% of the ocean kinetic energy (Richardson, 1983; Klein et al., 2019). At 1° (coarse resolution), mesoscale eddies are not permitted and need to be parameterized. At 1/10° (eddying resolution), there is a reasonable representation of the mid-latitude western boundary currents and associated mesoscale eddies (e.g., Paiva et al., 1999; Smith et al., 2000; Hallberg, 2013) and their impacts on large-scale circulation in global/basin scale simulations is now well-recognized (e.g., Chassignet et al., 2020; Hirschi et al., 2020; Roberts et al., 2020). When the horizontal grid spacing approaches 1 km (sub-mesoscale enabling resolution), ocean models not only resolve mesoscale eddies, but also start to resolve some sub-mesoscale features at mid- and low-latitudes. The impact of resolving sub-mesoscale variability on large-scale ocean circulation has been highlighted by Hurlburt and Hogan (2000), Lévy et al. (2010), Chassignet and Xu (2017), and Chassignet et al. (2023).

In contrast to the rich literature quantifying the impact of the

☆ A manuscript submitted to Ocean Modelling.

* Corresponding author.
E-mail address: xxu3@fsu.edu (X. Xu).

https://doi.org/10.1016/j.ocemod.2023.102261
Received 2 April 2023; Received in revised form 31 July 2023; Accepted 25 August 2023
Available online 26 August 2023

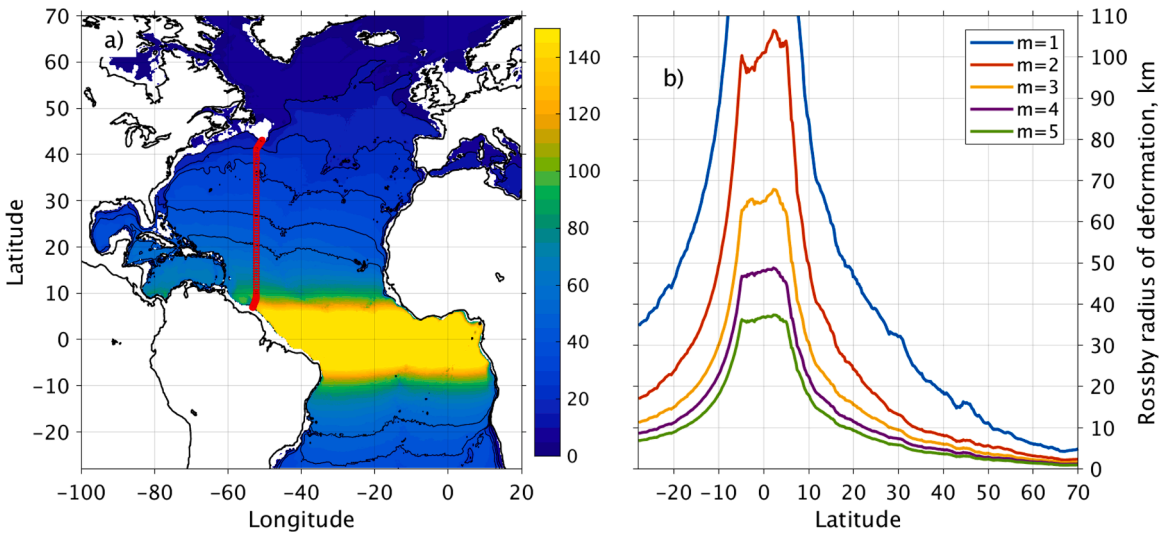

Fig. 1. (a) First baroclinic Rossby radius of deformation (in km) in the North and Equatorial Atlantic Ocean as computed from the density profiles of the ocean climatology-generalized digital environment model (GDEM, Carnes 2009). The black contours in the North Atlantic from south to north are 50, 40, 30, 20, and 10 km, respectively. The red circles indicate location of the WOCE line A20 along which high-resolution hydrographic surveys are conducted. (b) Zonally averaged Rossby radii for the first five baroclinic modes.

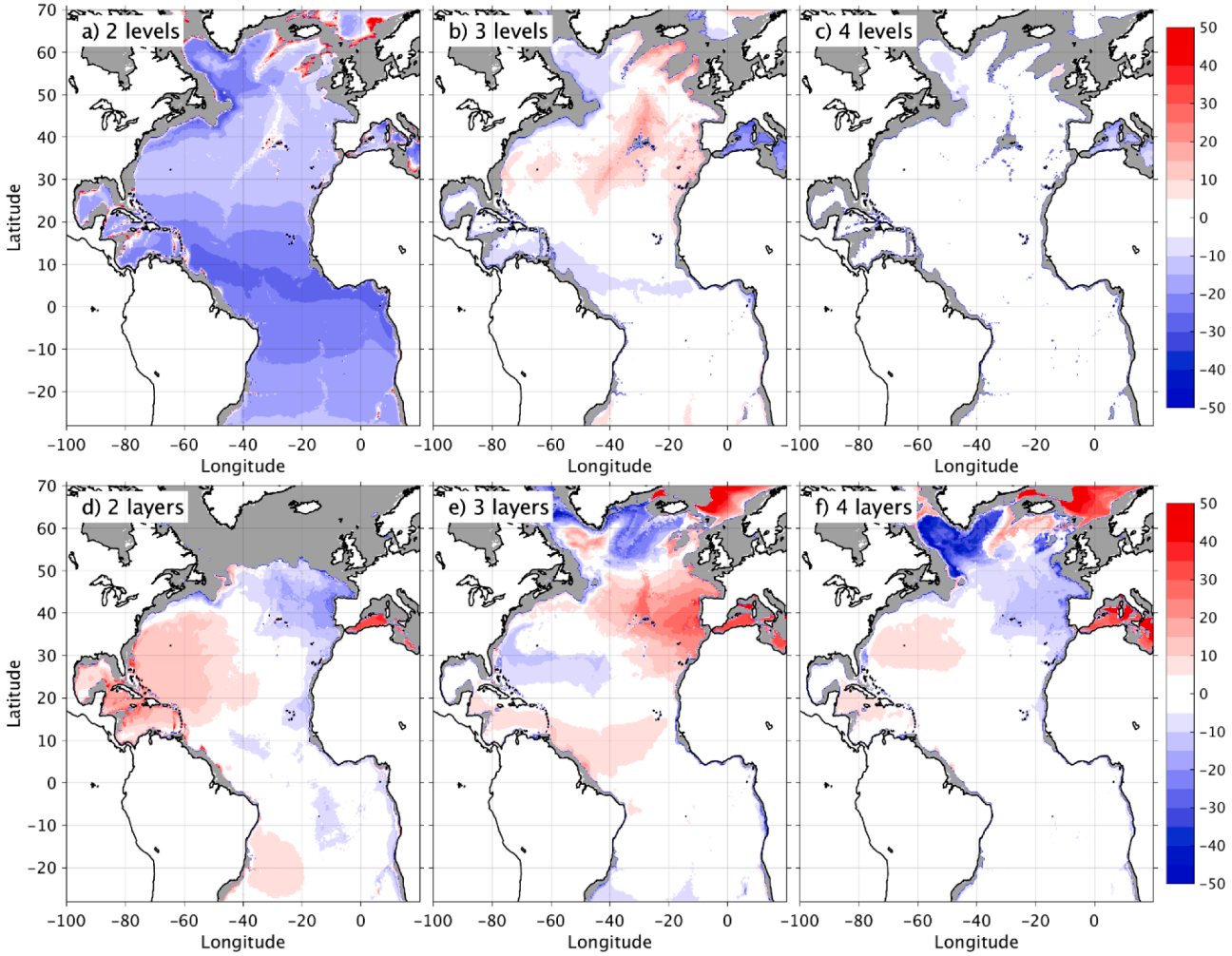

Fig. 2. Error (in%) in the first Rossby radius of deformation calculated from 2, 3, and 4 levels (a-c) and 2, 3, 4 isopycnic layers (d-f) when compared to the Rossby radius of deformation calculated from GDEM4 climatology. Blue/red color indicates where the low vertical resolution configuration under-/overestimates the first Rossby radius. Gray areas indicate regions where the Rossby radius cannot be computed (depth too shallow or non-existing density). Levels and layer densities are provided in Tables A1 and A2 of the Appendix.

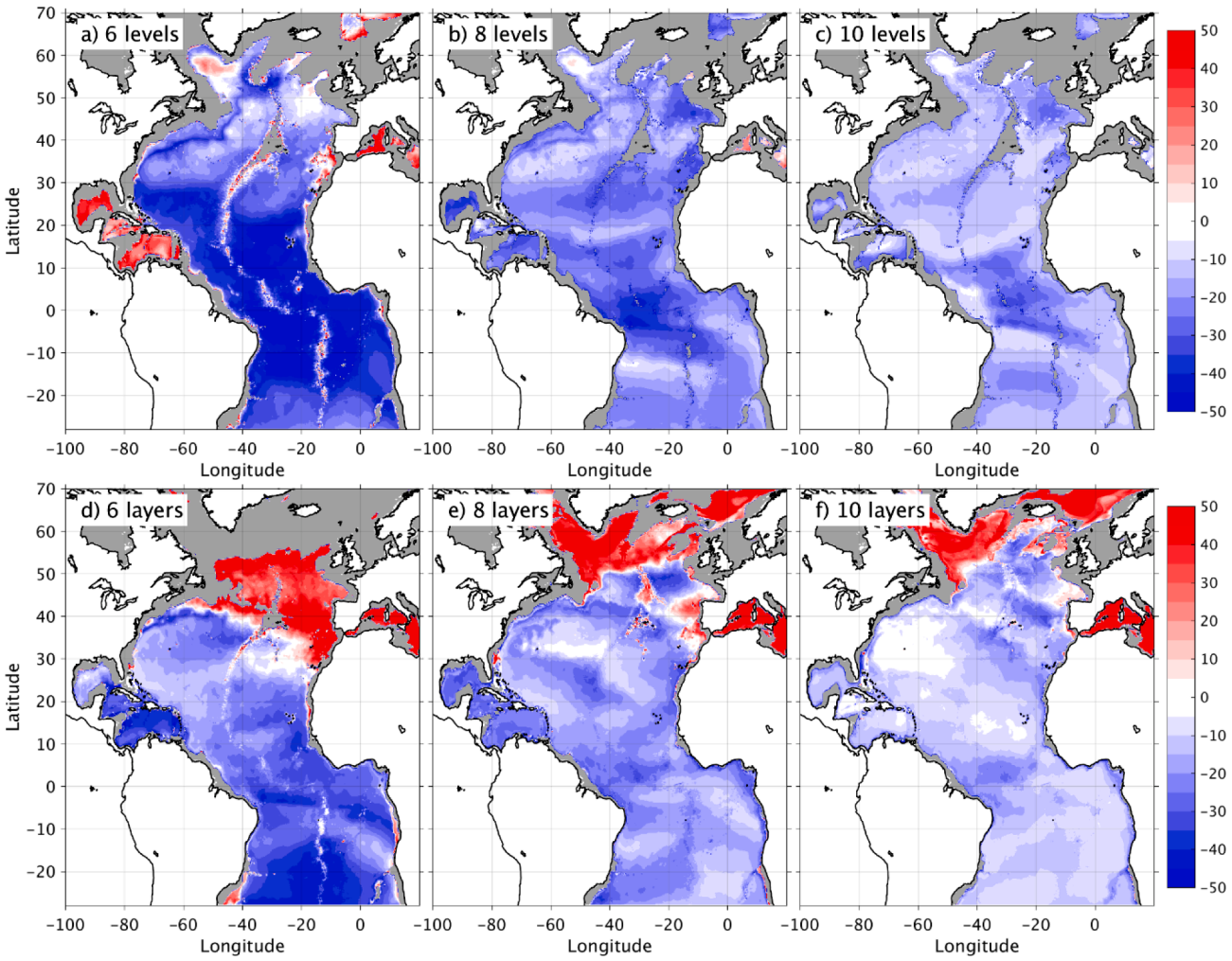

Fig. 3. Difference (in%) between the fifth Rossby radius of deformation calculated from GDEM, from 6, 8, and 10 levels (a-c), and 6, 8, and 10 isopycnic layers (d-f). Blue/red color indicates where the low vertical resolution configuration under-/over-estimates the fifth Rossby radius of deformation. Gray areas indicate regions where the Rossby radius cannot be computed (depth too shallow or non-existing density). Levels and layer densities are provided in Tables A1 and A2 of the Appendix.

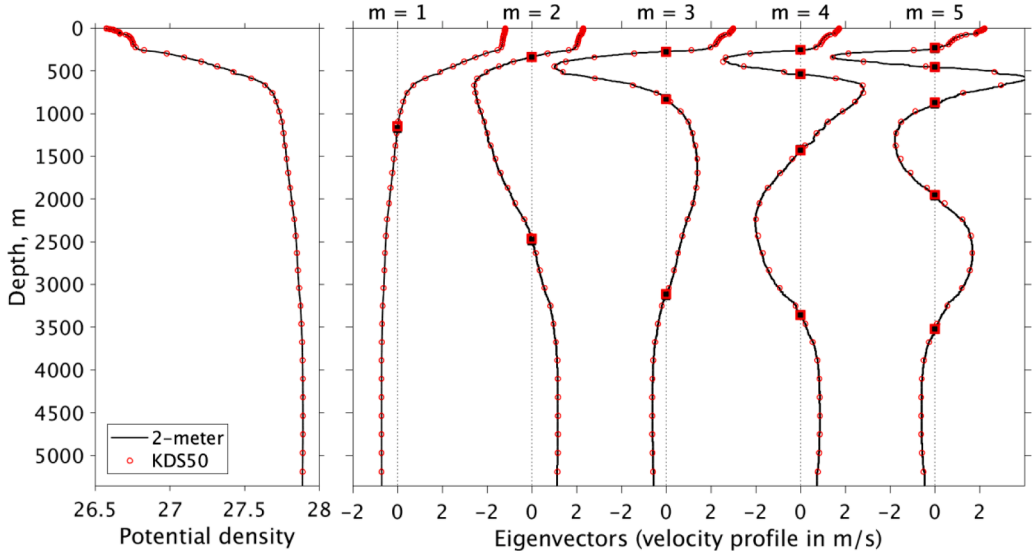

Fig. 4. (Left panel) potential density profile of potential density at a station near 40°N along the WOCE line A20 (red circles in Fig. 1), black line is of 2 m resolution and red-circle is in KDS50 grid in Stewart et al. (2017), with 53 levels from 2.7 m near surface to 219 m at a maximum depth of 5363 m. (Right panel) the corresponding velocity profile of the first five baroclinic modes based on 2 m resolution (black line) and KDS50 grid (red circles), with zero-crossing depth marked by squares for the 2 m resolution (black) and the KDS50 grid (red).

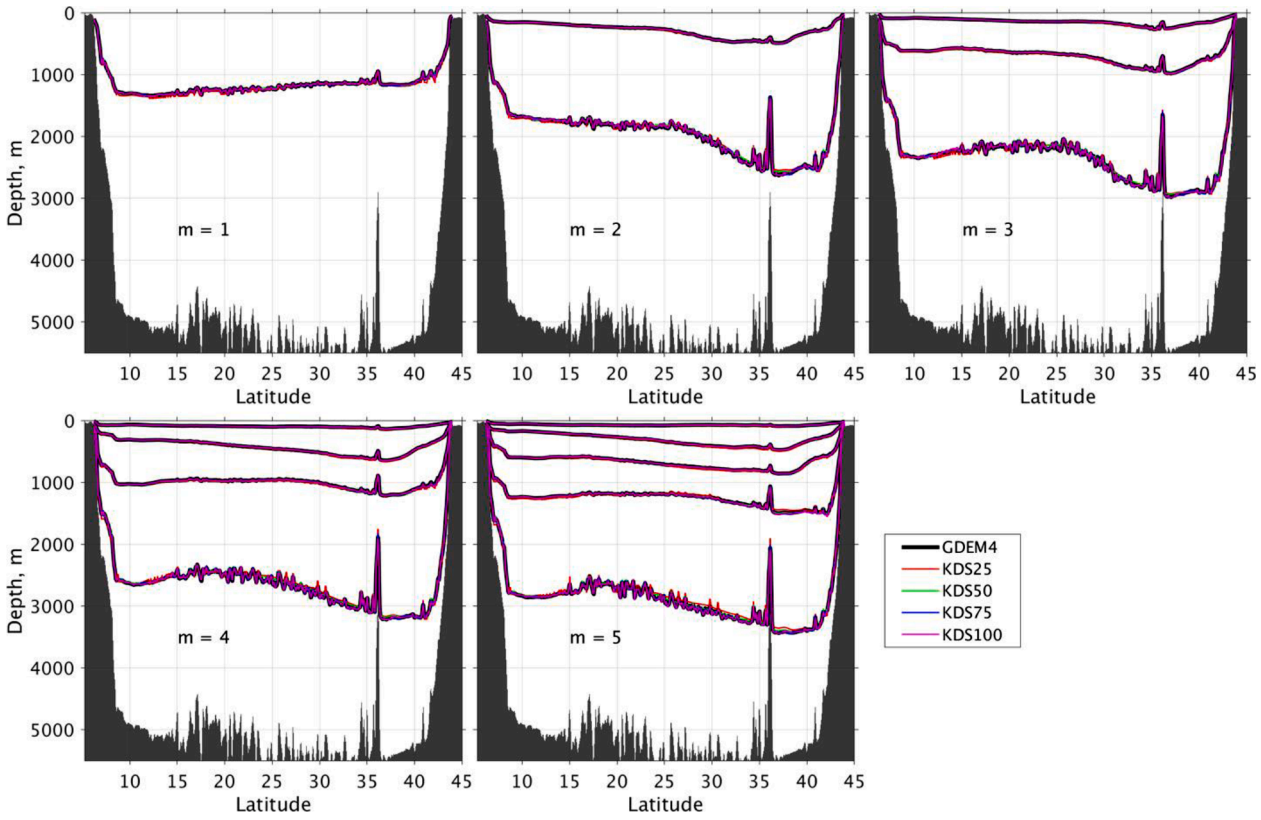

Fig. 5. Zero-crossing depth of the first five baroclinic modes along 52°W based on the ocean climatology GDEM (black lines) and four z-levels configurations with KDS25 (red), KDS50 (green), KDS75 (blue), and KDS100 (magenta).

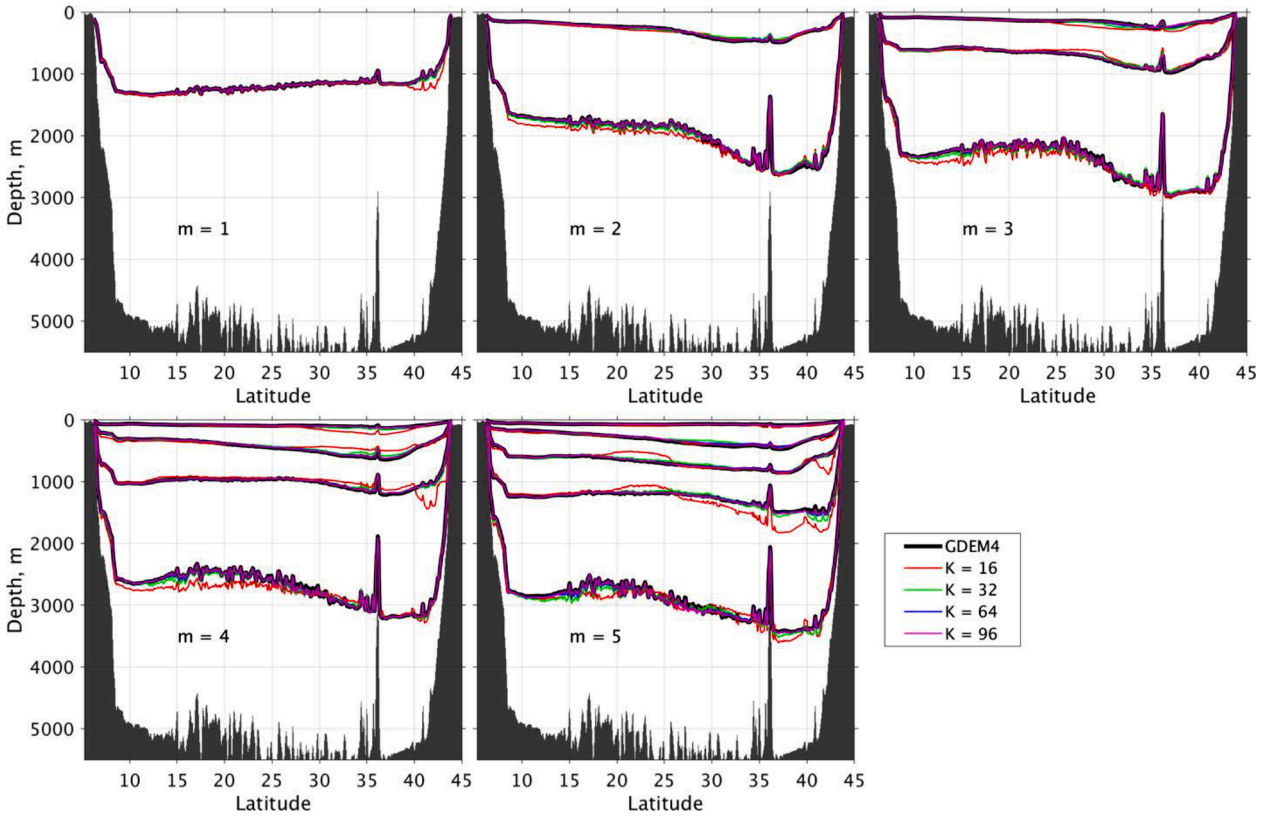

Fig. 6. Zero-crossing depth of the first five baroclinic modes along 52°W based on the ocean climatology GDEM (black lines) and four isopycnic configurations with 16 (red), 32 (green), 64 (blue), and 96 (magenta) layers.

Table 1
The average error (in%) of the zero-crossing depth along A20. The error is defined as the normalized difference between the zero-crossing depth as calculated from the GDEM4 resolution and from OGCMs grids: four z-level configurations (KDS25, KDS50, KDS75, and KDS100) and four layer configurations with 16, 32, 64, and 96 layers.

	$m = 1$	$m = 2$	$m = 3$	$m = 4$	$m = 5$
KDS25	2.1	2.9; 1.7	4.1; 2.0; 1.6	5.7; 2.2; 1.7; 1.7	7.4; 4.0; 2.3; 1.7; 1.8
KDS50	0.8	0.8; 1.1	1.1; 0.7; 1.1	1.5; 0.8; 0.6; 1.0	1.5; 0.8; 0.7; 0.6; 0.8
KDS75	0.7	0.7; 0.7	1.1; 0.7; 0.7	1.2; 0.7; 0.6; 0.6	1.0; 0.8; 0.7; 0.6; 0.5
KDS100	0.5	0.6; 0.6	0.8; 0.6; 0.5	0.9; 0.7; 0.4; 0.4	0.7; 0.9; 0.6; 0.6; 0.4
$K = 16$	3.2	8.8; 4.8	22.6; 5.8; 3.5	31.6;11.9; 7.3; 4.4	18.3; 8.1; 8.2; 9.7; 3.5
$K = 32$	0.6	5.1; 1.9	8.1; 2.0; 1.5	7.3; 4.4; 1.4; 1.4	5.2; 5.5; 3.0; 2.6; 1.8
$K = 64$	0.2	2.2; 0.6	2.5; 0.8; 0.5	3.1; 1.8; 0.5; 0.5	4.5; 4.0; 1.2; 0.8; 0.7
$K = 96$	0.3	1.5; 0.4	2.0; 0.8; 0.4	3.1; 1.4; 0.4; 0.3	4.3; 2.7; 0.8; 0.7; 0.5

horizontal resolution on ocean circulation, few studies have discussed the impact of vertical resolution. The early studies (Adamec, 1988; Weaver and Sarachik, 1990; Barnier et al., 1991) were performed with either a quasi-geostrophic model or OGCMs with relatively low vertical resolution. The importance of vertical resolution was revisited recently by Stewart et al. (2017) who state that the purpose of the vertical grid in a hydrostatic OGCM is to resolve the vertical structure of the horizontal flows (rather than to resolve vertical motions), and that vertical grids should be constructed to represent baroclinic modal structures to complement and not undermine the theoretical capabilities of a given horizontal grid. Stewart et al. (2017) suggest that for z-coordinate global ocean models, at least 50 well-positioned vertical levels are required to resolve the first baroclinic mode, with an additional 25 levels per subsequent mode. They showed that, when vertical resolution is increased from 50 to 75 levels, a 1/10° global ocean simulation gains some dynamical enhancements, including substantial increases in the sea surface height (SSH) variance and eddy kinetic energy (EKE) as well as in the magnitude of the overturning streamfunction associated with the Antarctic Bottom Water (AABW).

It is, however, important to point out that the increases in SSH variance/EKE and overturning strength in Stewart et al. (2017) when using 75 levels are most noticeable in the southern high latitudes (see their Figs. 9 and 10) where the 1/10° horizontal resolution only partially resolves the first baroclinic mode (Hallberg, 2013) and does not resolve the second baroclinic mode. Furthermore, a recent study by Ajayi et al. (2020, 2021) show that having "only 32 isopycnal layers was not detrimental to the representation of the dynamics in the ocean interior" when comparing two sub-mesoscale enabled North Atlantic simulations with drastically different vertical resolutions: one 1/60°, 300-level NEMO (a z-level model) and the other 1/50°, 32-layer HYCOM (a hybrid coordinate ocean model with isopycnic coordinates in the stratified interior). A comparison of the vorticity spectral coherence as a function of depth showed that the two simulations are essentially identical in terms of the depth penetration of energetic eddy structures. Besides resolving baroclinic modes, the vertical resolution in OGCMs serves another fundamental purpose, i.e. an accurate representation of water masses and associated water mass transformation. The question then arises as to whether the dynamical enhancements of Stewart et al. (2017) are indeed truly due to a better representation of the second baroclinic mode with the additional 25 levels or to the addition of levels that better discretize the high latitude water masses and allow for more

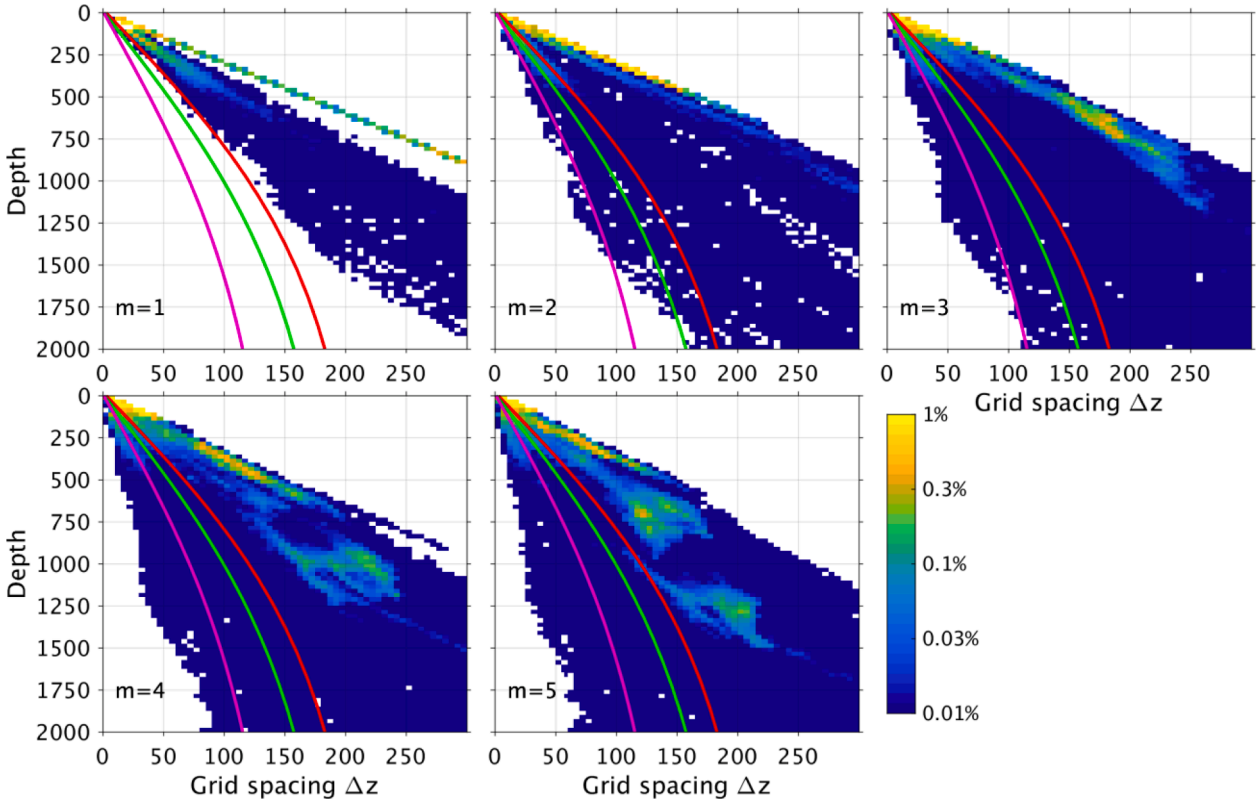

Fig. 7. Probability distribution (color shading) of the grid spacing Δz needed to resolve the first five baroclinic modes in the Atlantic Ocean as a function of depth compared to the vertical grid defined for KDS50 (red), KDS75 (green), and KDS100 (magenta) as defined in Stewart et al. (2017). To fully resolve the baroclinic mode, there should be no Δz distribution to the left of the colored lines.

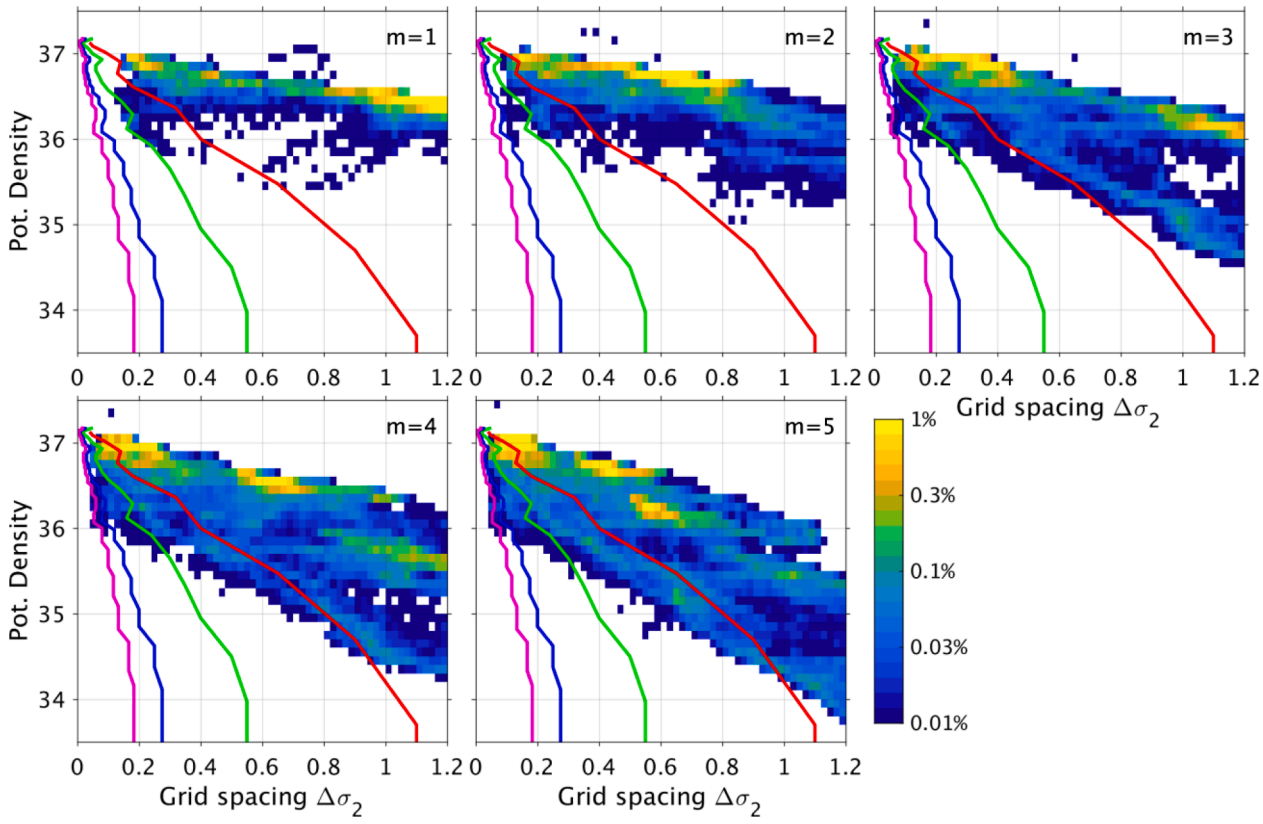

Fig. 8. Probability distribution (color shading) of the density spacing (in σ_2) needed to resolve the first five baroclinic modes in the Atlantic Ocean as a function of potential density, compared to the vertical density grid defined for 16 (red line), 32 (green line), 64 (blue line), and 96 (magenta line) layers. To fully resolve the baroclinic mode, there should be no density spacing distribution to the left of the colored lines.

accurate dense water formation (i.e., the AABW in Stewart et al. (2017)).

In this paper, we document and quantify the impact of the vertical resolution on the ocean circulation and water mass representation when using both z-levels and constant density layers (i.e., isopycnals) as the vertical coordinate. The main difference between *z*-level and layer (isopycnal) models is the ability of the latter to differentiate and keep track of distinct water masses, with the caveat that potential density surfaces are not exactly neutral, especially in high latitudes (see Stanley, 2019 for discussion on neutral surface). First, in Section 2, we argue that vertical resolution is unlikely to undermine the capability of a given horizontal grid in representing the vertical modes. Both the 50 well-positioned *z* levels as in Stewart et al. (2017) and the standard 32-layer HYCOM configuration are adequate choices to represent the zero-crossing of first five baroclinic modes in mid-latitudes as well their vertical structure. Subsequently, in Section 3, we investigate the impact of the vertical resolution choices on water mass representation and the circulation in a series of 1/12° North and Equatorial Atlantic configurations using isopycnic coordinates. Specifically, we find that the 24-, 32-, 64-, and 96-layer configuration all exhibit similar large-scale North Atlantic surface circulation and Atlantic meridional overturning circulation, whereas the 16-layer simulation is unable to accurately represent dense overflow waters. These findings are summarized, and their implications are discussed in Section 4.

2. Vertical mode representation in *z*-level and isopycnic coordinates

2.1. Horizontal resolution and the baroclinic rossby radii of deformation

Before discussing how a specific baroclinic mode is resolved by the vertical grid, it is useful to first review the minimum horizontal grid spacing that is needed to resolve the corresponding baroclinic Rossby radius of deformation (Rossby radius hereafter) and associated physical processes in an OGCM. Fig. 1 displays the spatial distribution of the first baroclinic Rossby radius in the North and Equatorial Atlantic Ocean computed from the annual mean density profiles of an ocean climatology (Chelton et al., 1998), and the zonally averaged Rossby radii for the first five baroclinic modes as a function of latitude. The Rossby radius and the vertical structure of the baroclinic modes are obtained by solving a Sturm-Liouville eigenvalue problem (e.g., Chelton et al., 1998; Hallberg, 2013; Stewart et al., 2017) with the Rossby radius, λ_m, for mode-*m* defined as

$$\lambda_m = \sqrt{\frac{c_m^2}{(f^2 + 2\beta c_m)}} \tag{1}$$

and the corresponding baroclinic wave phase speed, c_m, defined as

$$c_m \approx \frac{1}{m\pi} \int_{-H}^{0} N(z)dz. \tag{2}$$

f and β are the Coriolis parameter and its meridional derivative, respectively, and $N(z)$ is the Brunt-Väisälä frequency.

The first Rossby radius is in the order of 20–40 km at mid-latitude, but decreases to less than 10 km in the subpolar North Atlantic because of an increasing Coriolis parameter and decreasing stratification. If we assume that a minimum of two grid points is needed within the Rossby radius to resolve the first baroclinic mode, i.e., Hallberg (2013), thus, an eddying resolution of 1/12° (~6 km) does resolve the first baroclinic mode at mid-latitudes, but barely in the weakly stratified high latitude ocean. However, if we adopt Soufflet et al. (2016)'s concept of an effective resolution which depends on the OGCM's inherent numerical dissipation which is on the order of 6Δx, then 1/12°

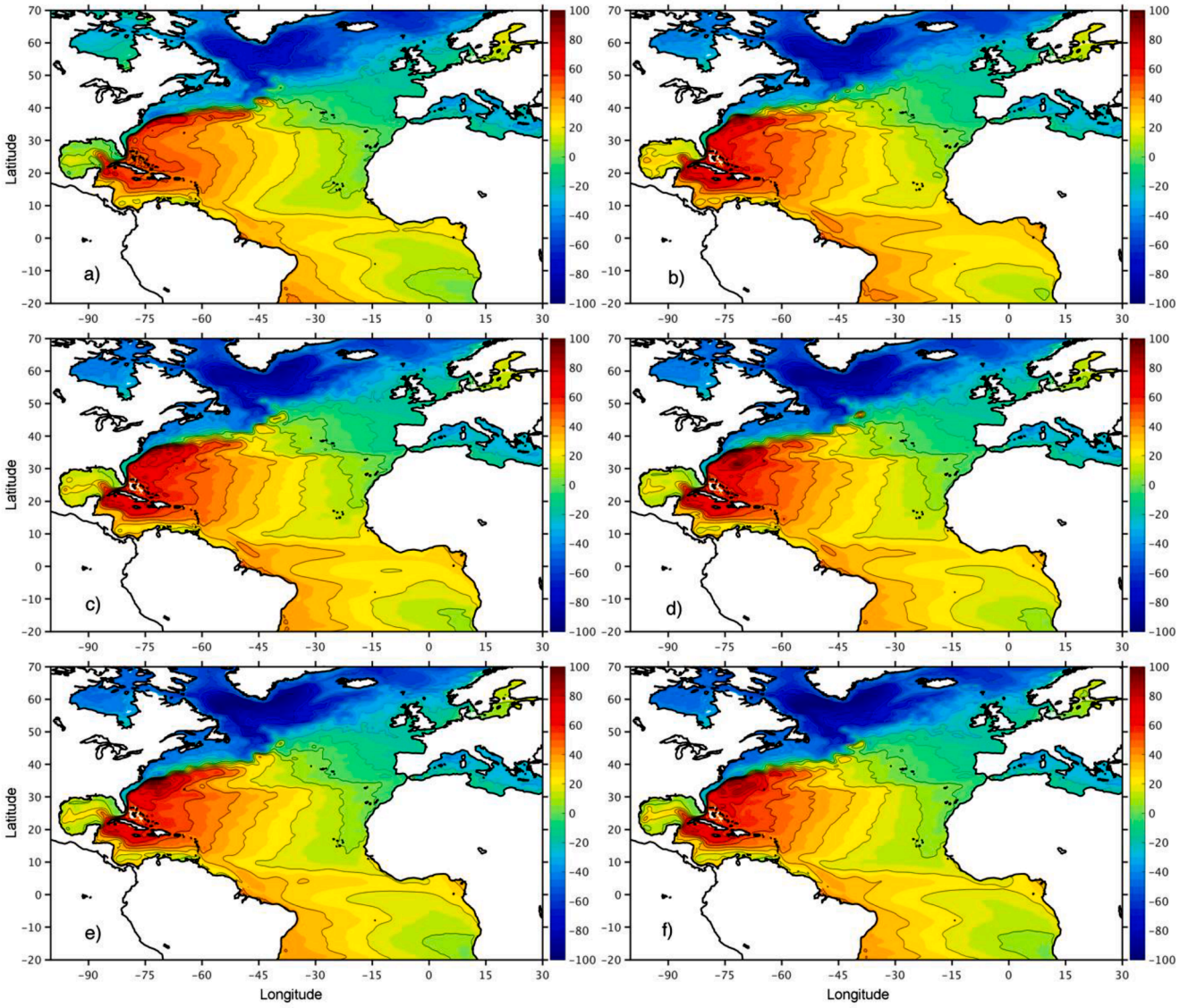

Fig. 9. A comparison of observed and modeled time mean surface circulation: a) the CNES_CLS18 mean dynamic topography MDT (in cm, from Mulet et al., 2021), b-f) the 5-year mean modeled sea surface height (SSH, in cm) from five 1/12° Atlantic HYCOM simulations with 16, 24, 32, 64, and 96 layers, respectively.

(~6 km) barely resolves the first baroclinic mode at mid-latitudes. Considering that 1/50° (~1.5 km) represents the finest horizontal resolution currently used in OGCMs (Uchida et al., 2022) and that the Rossby radius for the m^{th} baroclinic mode is approximately the first baroclinic Rossby radius divided by m, current sub-mesoscale enabled OGCMs are only able to resolve up to the fifth baroclinic Rossby radius at mid-latitudes if one adopts Hallberg (2013)'s 2Δx criterion and even less with Soufflet et al. (2016)'s 6Δx criterion. Subsequently, in the remainder of this paper, we focus only the representation of the first five baroclinic modes.

2.2. Vertical resolution and the baroclinic rossby radii of deformation

In theory, the first baroclinic mode for a given density profile can be represented as a two-layer system with one zero-crossing interface. Thus, over a given domain, it is reasonable to expect that only a few z-levels or density layers should be able to provide a reasonable representation of the first Rossby radius, provided that the spatial variation of the density and corresponding interface depth are small. We test this hypothesis over the North and Equatorial Atlantic by computing the first Rossby radius using (a) 78-level GDEM climatology (Fig. 1a) as the reference, (b) 2, 3, and 4 fixed z-levels (derived from the spatially averaged zero-crossing depths of the 1st, 2nd, and 3rd baroclinic mode, respectively), and (c) 2, 3, and 4 isopycnic layers (derived from the spatially averaged densities above and below the zero-crossing depths of the 1st, 2nd, and 3rd baroclinic mode, respectively). Fig. 2 shows the error in the first Rossby radius, $E(R_m)$, calculated using 2 to 4 levels or layers when compared to that of calculated from the 78-level climatology (Fig. 1a).

$$E(R_m) = \frac{R_m^{low} - R_m^{clim}}{R_m^{clim}}, \tag{3}$$

in which R_m^{clim} is the Rossby radius for mode m calculated from 78-level GDEM climatology (Fig. 1a), and R_m^{low} from the lower vertical resolution configurations. A minimum of 2 levels or layers is required to compute the first baroclinic Rossby radius. When two levels are defined using the spatially averaged zero-crossing depth of the first mode (1170 m, see Table A1 in the Appendix), the error in the first Rossby radii is on the order of 10% to 20% over most of the domain and is higher in the tropics (Fig. 2a). It is significantly less when using 2 isopycnic layers (σ_2 densities of 35.80 and 36.96 kg/m^3, see table A2 in the Appendix) (Fig. 2d),

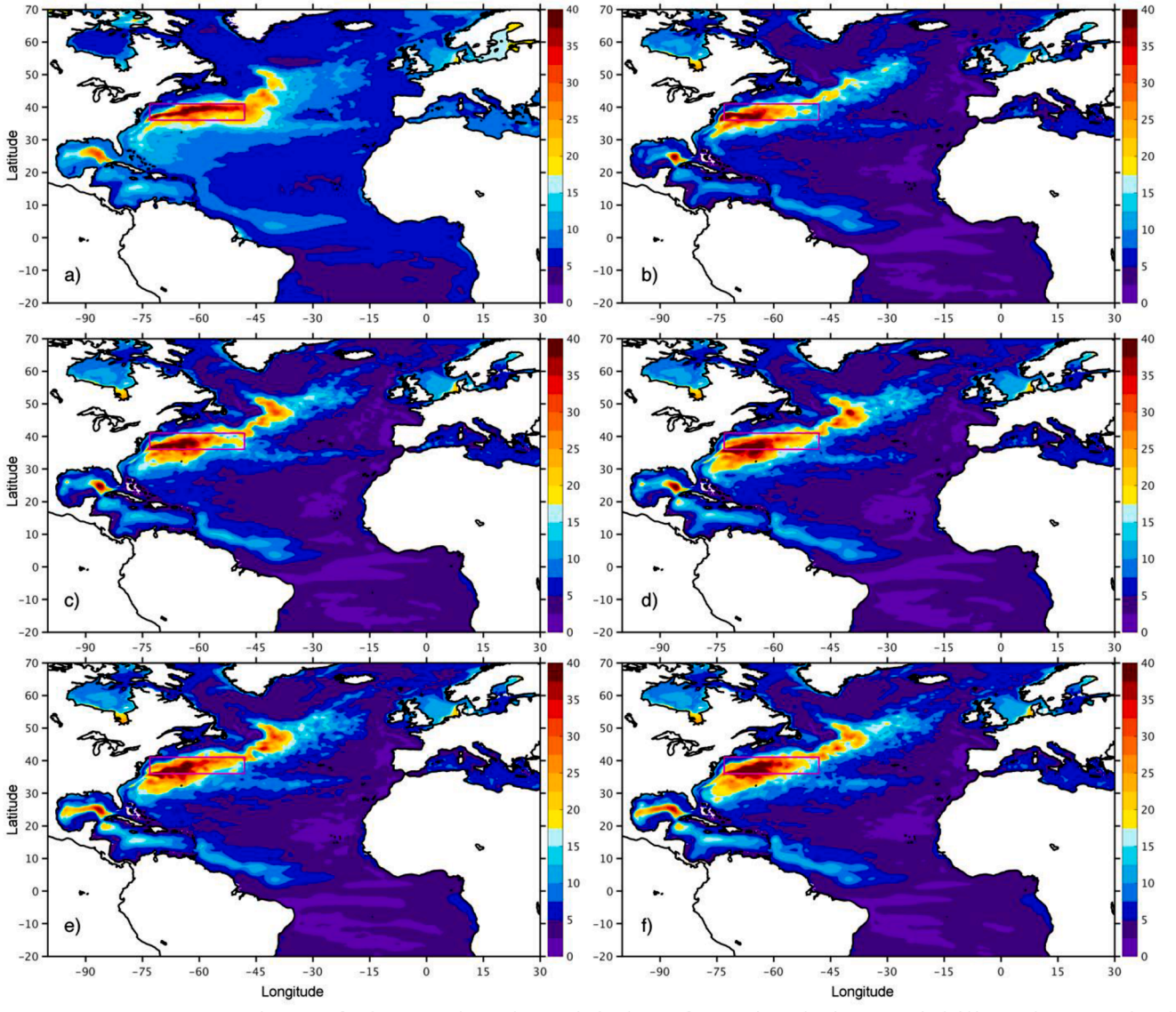

Fig. 10. A comparison of observed and modeled surface circulation variability: the standard deviation value of the sea surface height (SSH, in cm) from a) satellite altimetry data (1993–2018) distributed by Copernicus Maine Environment Monitoring Services (CMEMS) and b-f) five 1/12° Atlantic HYCOM simulations with 16, 24, 32, 64, and 96 layers, respectively.

especially in the tropics. The main reason is that for most of the Equatorial/mid-latitude region, a 2-layer configuration defined by the permanent pycnocline is a good approximation of the density profile. It does not perform as well at higher latitudes in unstratified regions. As one increases the number of levels or layers, the error in the Rossby radius drops quickly and, in the Equatorial/mid-latitude region, it is very small (less than 5%) with 4 levels or 4 layers.

One can repeat this exercise for higher modes. Fig. 3 displays the error in the fifth Rossby radii calculated for 6, 8, and 10 levels and 6, 8, and 10 layers, respectively (the z-levels and isopycnic layer densities are listed in the Appendix in Tables A1 and A2), when compared to the Rossby radii calculated from the GDEM climatology. A minimum of 6 levels/layers is required to compute the fifth Rossby radius and the percentage error is higher (on the order of 50% for the z-levels, less for the layer configuration) than for the first Rossby radius defined by 2 levels/layers (Fig. 2). As for the first Rossby radius (Fig. 2), the error also decreases as the vertical resolution increases, but at a slower pace. With 10 levels/layers, the error is in the order of 15–20%.

Overall, the results shown in Figs. 2 and 3 confirm the premise that one does not require that many levels or layers to represent the first five Rossby radius over most of the deep ocean. This, however, does not mean that such a low-resolution vertical grid can be applied to a basin scale or global model. For example, one cannot define two levels in regions when the depth is less than the spatially averaged zero-crossing depth (or when density at bottom is lower than the spatially averaged density). These areas are shown in gray in Figs. 2 and 3. In addition, surface water is denser in high latitude than in the tropical region, thus some isopycnals (defined by spatially averaged density) outcrops to the surface in the subpolar region and the effective number of isopycnic layers is reduced (e.g., the unstratified regions in the subpolar North Atlantic). In the overflows, both coordinate systems fail to represent mode 1 processes.

2.3. *Baroclinic mode representation in OGCMs*

A proper representation of the baroclinic Rossby radii is a measure of how well the model can represent the phase speed of the first baroclinic mode or the total stratification of the water column using the WKB approximation (Chelton et al., 1998; Stewart et al., 2017) . In addition to ensuring that the vertical grid provides the right Rossby radii (focus of

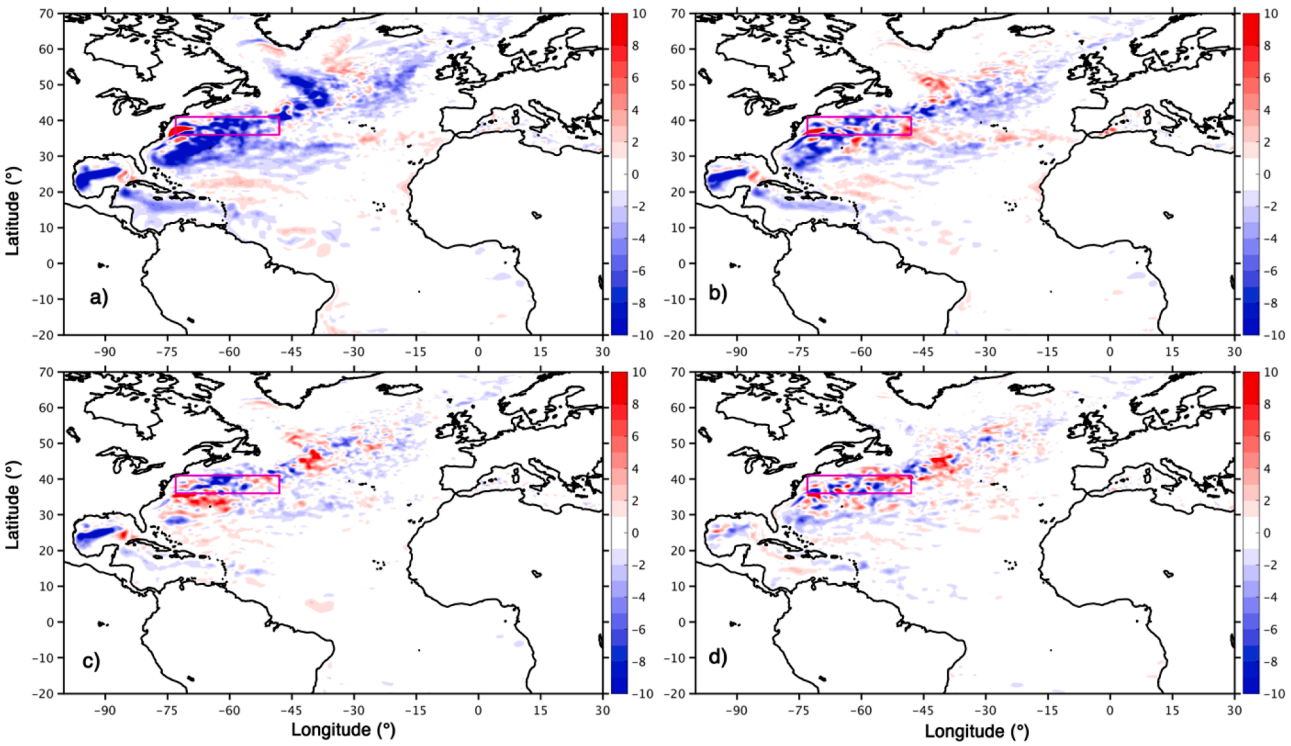

Fig. 11. Difference in the standard deviation of the sea surface height (SSH, in cm) in a) 16-layer, b) 24-layer, c) 32-layer, and d) 64-layer 1/12° Atlantic HYCOM simulations compared to the 96-layer HYCOM simulation. Blue color indicates lower SSH variability compared to 96-layer simulation.

the previous section), one could also argue that the vertical structure of the baroclinic modes themselves needs to be resolved (Stewart et al., 2017). In this section, we evaluate the ability of vertical grids commonly used in OGCMs to do so. The left panel of Fig. 4 shows a single density profile near 40°N from the World Ocean Circulation Experiment (WOCE) line A20 where the black line is the original 2-m resolution CTD data and the red circles represent the profile using the KDS50 grid of Stewart et al. (2017) (varying grid spacing from 2.7 m near the surface to 219 m near the bottom). The right panel shows the corresponding vertical profile of the first five baroclinic modes calculated from the 2 m resolution and the KDS50 grid, respectively. There is no loss of information when using the KDS50 grid for all five modes, with nearly identical velocity profile and zero-crossing depth (Fig. 4). Similar result can be found for other stations along the section.

To assess how well the vertical mode structure is represented in an OGCM grid, Fig. 5 displays the distribution of zero-crossing of the first five modes computed from the GDEM climatology and four z-levels configurations, KDS50, KDS75, and KDS100 in Stewart et al. (2017), and KDS25 that is defined as half of the resolution KDS50 (by merging every two levels into one). The results show that all four OGCM grid represent the zero-crossing well. One way of quantifying the differences is to calculate a normalized error, $\overline{E(h_{m,k})}$, as in Stewart et al. (2017) in zero-crossing depths between the climatology and the OGCMs' vertical grids.

$$\overline{E\left(h_{m,k}\right)} = \frac{\overline{\left|h_{m,k}^{clim} - h_{m,k}^{OGCM}\right|}}{h_{m,k}^{clim}}, \tag{4}$$

in which $h_{m,k}^{clim}$ and $h_{m,k}^{OGCM}$ are the depth of the k^{th} zero-crossing for the m^{th} mode as represented in climatology and in OGCM resolution, respectively. The averaged error for the full section is less than 10% for KDS25, and 2% for the other three grids. The small error is not too surprising as a hindsight, because the GDEM climatology itself is 78-level, thus the error in the KDS75 and KDS100 is essentially rounding error introduced by re-griding and interpolating.

The next step is to assess how well the vertical mode structure is represented in OGCMs with isopycnic coordinates. Fig. 6 displays the zero-crossing depths of the first five baroclinic modes along A20 line near 52°W represented in four configurations with 16, 32, 64, and 96 layers used in the North and Equatorial Atlantic HYCOM configuration. The standard 32-layer configuration has been used extensively by Xu et al. (2010, 2012, 2014, 2022), Chassignet and Xu (2017, 2021), and Chassignet et al. (2023). The selection of isopycnic layers was adapted from a previous global simulation and was modified to represent the key water masses in the Atlantic Ocean, especially the deep dense water masses (see Xu et al., 2012). The 16, 64, and 96 layers were constructed by either collapsing layers or splitting the layers in two or three from the original 32-layer configuration. The 16-layer configuration represents the first and second modes reasonably well, but not the higher modes (Fig. 6) in part because of its shallower first interface depth (Eq. (4)), whereas the 32, 64, and 96-layer configurations represent the zero-crossing depths of all five modes to a good approximation. The normalized errors along the A20 section for all 15 zero-crossing depth of the first five modes are less than 10% for the 32-layer configuration and less than 5% for the 64 and 96-layer configurations (Table 1).

2.4. *Vertical grid spacing requirements in z-levels versus isopycnic layers*

Stewart et al. (2017) evaluates the ability of a vertical grid to represent the vertical modes by comparing the distribution of the model vertical grid spacing against the Δz requirement to resolve a specific mode. The latter is defined as 1/3 of the distance between zero-crossing depths in order to have a minimum of 3 grid points (see their Fig. 6). Fig. 7 reproduces Fig. 6 of Stewart et al. (2017), but for the first 5 modes and for the GDEM climatology in the North and Equatorial Atlantic. As in Stewart et al. (2017), we find that, for the first mode, all vertical grid spacing profiles (KDS50, KDS75, and KDS100) lie to the left of the data points, therefore meeting the resolution requirements (Stewart et al., 2017). For the second mode, only the 100-level vertical grid profile lies to the left. For the third, fourth, and fifth modes, there are some data lies

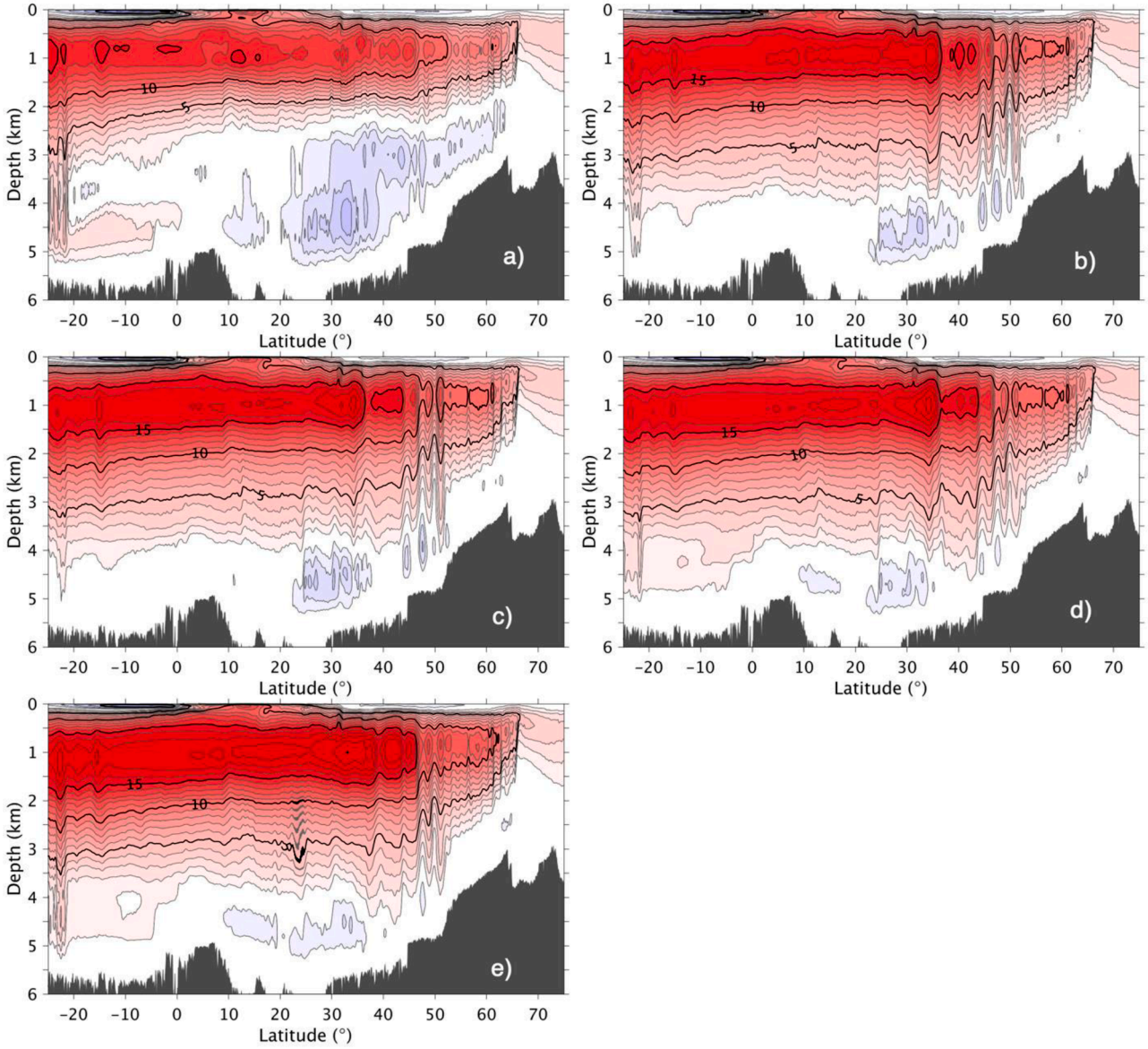

Fig. 12. Modeled time mean meridional overturning streamfunction (in Sv) as a function of depth (z) and latitude in five 1/12° Atlantic HYCOM simulations with different vertical resolutions: (a) 16, (b) 24, (c) 32, (d) 64, and (e) 96 layers, respectively. The results show that expect the 16-layer simulation, the other four simulations have an overall similar overturning streamfunction structure. .

to the left of the profile, but they only represent a small fraction of the total. We can repeat the same exercise, but this time in density space (Fig. 8). The 16-layer configuration meets most of the first and second modes requirements, but there is quite some data points lying to the left of the profile for the higher modes. The second mode is well represented with 32 and higher number of layers, but one would need 64 or 96 layers to fully satisfy the requirements of the third and higher modes.

In summary, we argue that the vertical resolution used in current OGCMs (50–75 levels or 30–40 layers) adequately represents the first two modes (zero-crossing depths and vertical grid requirement), but that there is definitely an advantage in using density layers instead of levels in representing higher modes. A 100-level configuration cannot satisfy Stewart et al. (2017)'s grid requirement for the first five modes while a 96-layer configuration does. This is primarily because a minimum of three levels is required in z-coordinate model to represent a single water mass versus only one constant density layer in isopycnic coordinate models, thus giving a factor of three advantage to the latter. Isopycnic coordinate models are also not constrained by the vertical grid when representing the bottom bathymetry.

3. Impact of vertical resolution on water mass representation in the North Atlantic

Being able to represent vertical modes accurately in a OGCM is only one aspect of choosing a vertical grid. The other constraint is being able to model the different water masses present throughout the ocean as well as the associated water mass transformations. While this was not the main purpose of the Stewart et al. (2017) study as it focused on modes, they did however include some water mass considerations when constructing their vertical grid (i.e., the minimum and maximum thickness near the surface and bottom). In this section, we not only investigate the impact of the vertical resolution on the ocean circulation from a baroclinic modal decomposition point of view, but also from a water mass representation perspective. This is achieved by performing a series of North and Equatorial Atlantic numerical simulations (28°S to 80°N) with varying vertical and horizontal grid spacing. The main reason for focusing on the North Atlantic is that the domain size is much more affordable computationally than the global domain, therefore allowing for the exploration vertical grid sensitivity over a wide range

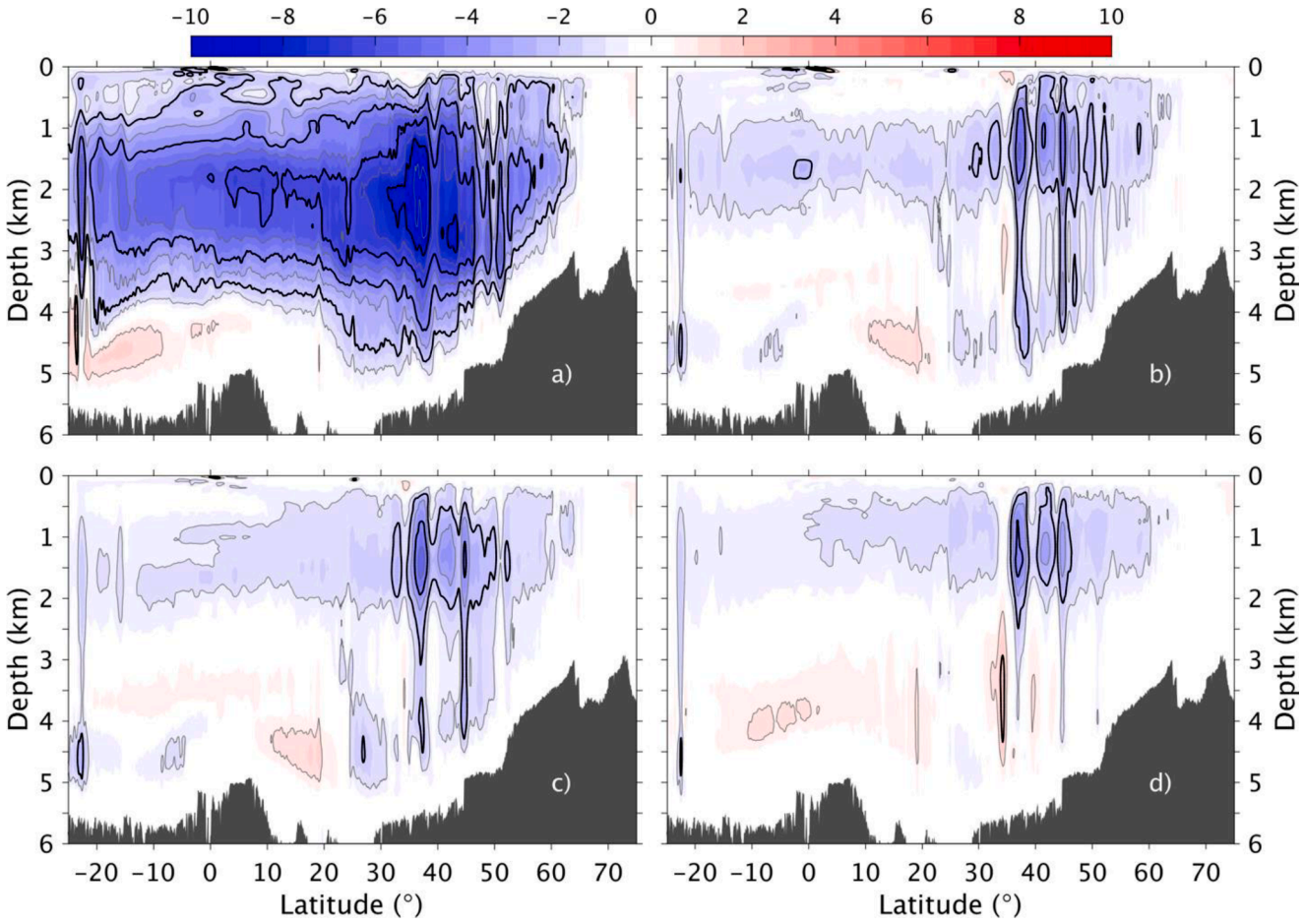

Fig. 13. Difference in modeled time-mean meridional overturning streamfunction (in Sv) as a function of depth and latitude in four 1/12° Atlantic HYCOM simulations with (a) 16, (b) 24, (c) 32, and (d) 64 layers, respectively, compared to the 96-layer simulation as a reference. Blue color indicates streamfunction value is lower in the low-resolution simulation and vice versa. The gray and black contours are with 1 and 2 Sv interval, respectively.

(from 16 to 96 layers). Furthermore, the North Atlantic is one of the most observed ocean basins (e.g., Frajka-Williams et al., 2019; Lozier et al., 2019), an important consideration when evaluating the realism of the model solutions. All simulations are performed with the Hybrid Coordinate Ocean Model (HYCOM; Bleck, 2002; Chassignet et al., 2003), in which the vertical coordinate is isopycnic in the stratified open ocean and makes a dynamically smooth and time-dependent transition to terrain following in shallow coastal regions and to fixed pressure levels in the surface mixed layer and/or unstratified seas. In doing so, the model combines the advantages of the different coordinate types in simulating coastal and open ocean circulation features simultaneously (Chassignet et al., 2006). The North and Equatorial Atlantic configuration is well documented; see Chassignet and Xu (2017) and the references therein. Details of the model configurations are provided in the Appendix.

3.1. *Time mean and variability of the surface circulation*

The time mean sea surface height (SSH) and its variability are displayed in Figs. 9 and 10, respectively. Fig. 9a is the latest CNES-CLS18 mean dynamic topography (MDT, Mulet et al., 2021), which is calculated from a combination of altimeter and space gravity data and oceanographic *in-situ* measurements (i.e., drifting buoy velocities, hydrographic profiles). The subtropical and subpolar gyres (represented by the sub-basin scale positive and negative anomalies, respectively), the western boundary current of the Florida Current, the Gulf Stream, and the North Atlantic Current (represented by the contracted MDT contours), as well as the Azores current near 35°N extended from 45°W to the Strait of Gibraltar can all be easily identified. The modeled circulation is similar to the observations from a large-scale perspective but differs in its details. The most noticeable difference between the observations and the model results is probably in the representation of the Gulf Stream and North Atlantic Current. At 1/12°, the modeled Gulf Stream does not extend far enough to the east and its southern recirculation is confined to the west of about 65°W (Chassignet and Xu, 2017). Among the five simulations, the 16-layer simulation (Fig. 9b) has the worst representation of the North Atlantic circulation with a northward Gulf Stream separation and a poor representation of the North Atlantic Current northwest corner near 52°N. The 16-layer simulation also has a weaker and shallower AMOC recirculation cell (discussed in the following section). Overall, the surface circulation in the other four simulations is similar to each other and an increase to 96 layers does not lead to a significantly change in surface circulation.

The kinetic energy of the ocean circulation is dominated by mesoscale eddies that are most active in the western boundary current system: the North Brazil Current, the Loop current, the Florida Current, the Gulf Stream, and the North Atlantic Current (Fig. 10a). While all five simulations represent this observed broad pattern well, there are some clear differences. Overall, the variability in the interior is lower in the models than in the observations. This is a common feature of models, even with finer horizontal resolution, which is attributed to the coarse resolution (space and time) atmospheric forcing (Chassignet and Xu, 2017; Chassignet et al., 2020). For the energetic western boundary current associated with the Gulf Stream, the modeled SSH variability has a wider area of high variability meridionally to the west of about 65°W and is weaker to the east of this longitude. As shown in Chassignet and

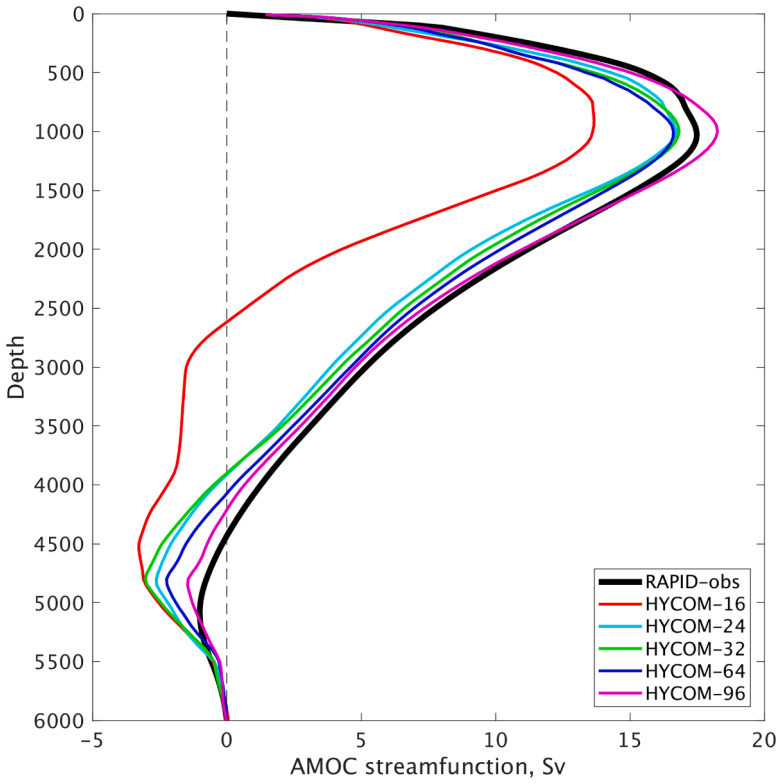

Fig. 14. Time mean meridional overturning streamfunction (in Sv) across the RAPID array near 26°N from observations and five 1/12° Atlantic HYCOM simulations with different vertical resolutions from 16 to 96 layers. The results show that expect the 16-layer simulation, the other four simulation show a similar overturning streamfunction as the observations.

Xu (2017), this is associated with the Gulf Stream not penetrating enough to the east at this resolution (1/12°) and the results are drastically improved when the horizontal resolution is increased to 1/50°. To provide a simple quantitative measure of the Gulf Stream SSH variability, we calculated the SSH standard deviation in a 25 × 5° box of 73–48°W, 36–41°N (magenta rectangle in Fig. 10). The area-averaged standard deviation value is 25.6 cm in observation (Fig. 10a), compared to 21.4, 23.7, 24.0, 24.9, and 25.2 cm for the five experiments of 16, 24, 32, 64, and 96-layer, respectively (Fig. 10b–f). The 10% increase from the 16- to the 24-layer simulation, although smaller than that in Stewart et al. (2017), may be representative of a better representation of the baroclinic mode as discussed in Section 2. The increase takes place in mid-latitude where the first Rossby radius is fully resolved by the 1/12° horizontal resolution. From 24 to 96-layer, the SSH variability continues to increase, but at a smaller pace, with a 6% increase in SSH variability for a 4-fold increase in the number of layers. The similarity or difference in modeled SSH variability is shown in Fig. 11, which displays the difference in SSH variability from the 16- to 64-layer configurations when compared to the 96-layer configuration. The 16-, 24- and, to a lesser degree, the 32-layer configurations clearly show a lower variability in the Gulf Stream and in the Gulf of Mexico, whereas the 64-layer configuration has a similar variability, when compared to the 96-layer reference. This is in general consistent with the point made in section that the baroclinic modes that are allowed by the horizontal resolution are better represented in the 64- and 96-layer simulations.

3.2. AMOC in the subtropical and subpolar North Atlantic

The AMOC consists of a northward flow of warm, saline water in approximately the upper 1 km and a southward flow of colder, fresher North Atlantic Deep Water below this depth (which is also roughly the depth of permanent pycnocline and hence the zero-crossing for the first baroclinic mode in the mid-latitude). Thus, it might be reasonable to expect some connections between the representation of the AMOC, the mode, and the vertical resolution. The large-scale AMOC is often defined by an overturning streamfunction ψ_z, which is calculated at a given latitude as the integrated meridional transport (Sv) across the basin from surface to a given depth z. The modeled streamfunction ψ_z as a function of latitude is shown in Fig. 12 for the five simulations: it shows a northward flow in the upper 1 km or so throughout the entire domain from the South Atlantic to about 60°N in the North Atlantic, and southward flow of North Atlantic Deep Water (NADW) below this depth. The most important result from Fig. 12 is that the AMOC structure is qualitatively similar in the four simulations with 24, 32, 64, and 96 layers, but that the 16-layer simulation exhibits a weaker AMOC with no southward flow below 2500 m, an indication of lacking dense overflow water contribution (which will be seen clearer in the streamfunction defined in density coordinate discussed later). The 24-layer simulation (Fig. 12b), which has the same upper layer distribution as in the 16-layer and a lower layer distribution as in the 32-layer, shows similar results to the 32-layer simulation (Fig. 12c). The difference in the modeled AMOC streamfunctions ψ_z is displayed in Fig. 13, with the 96-layer simulation used as a reference. The overturning strength increases with finer vertical resolution, with a maximum difference at mid-latitudes. The largest difference in streamfunction is more than 8 Sv for the 16-layer simulation when compared to the 96-layer, but this is reduced to 2–4 Sv in the other three simulations (24, 32, and 64 layers).

To compare the modeled AMOC structure and observations quantitatively, Fig. 14 displays the streamfunction ψ_z at 26.5°N. The black line from the updated RAPID line observations (e.g., Smead et al., 2018), and the colored lines represent the modeled streamfunction for the five simulations. The results highlight that, at this latitude, the 16-layer simulation has a weaker time-mean AMOC (14 versus 17 Sv) and that the southward component of NADW is too shallow (2600 versus 4500 m). The other four simulations have a time mean AMOC magnitude close to the observations (difference of about 1 Sv). As the vertical resolution

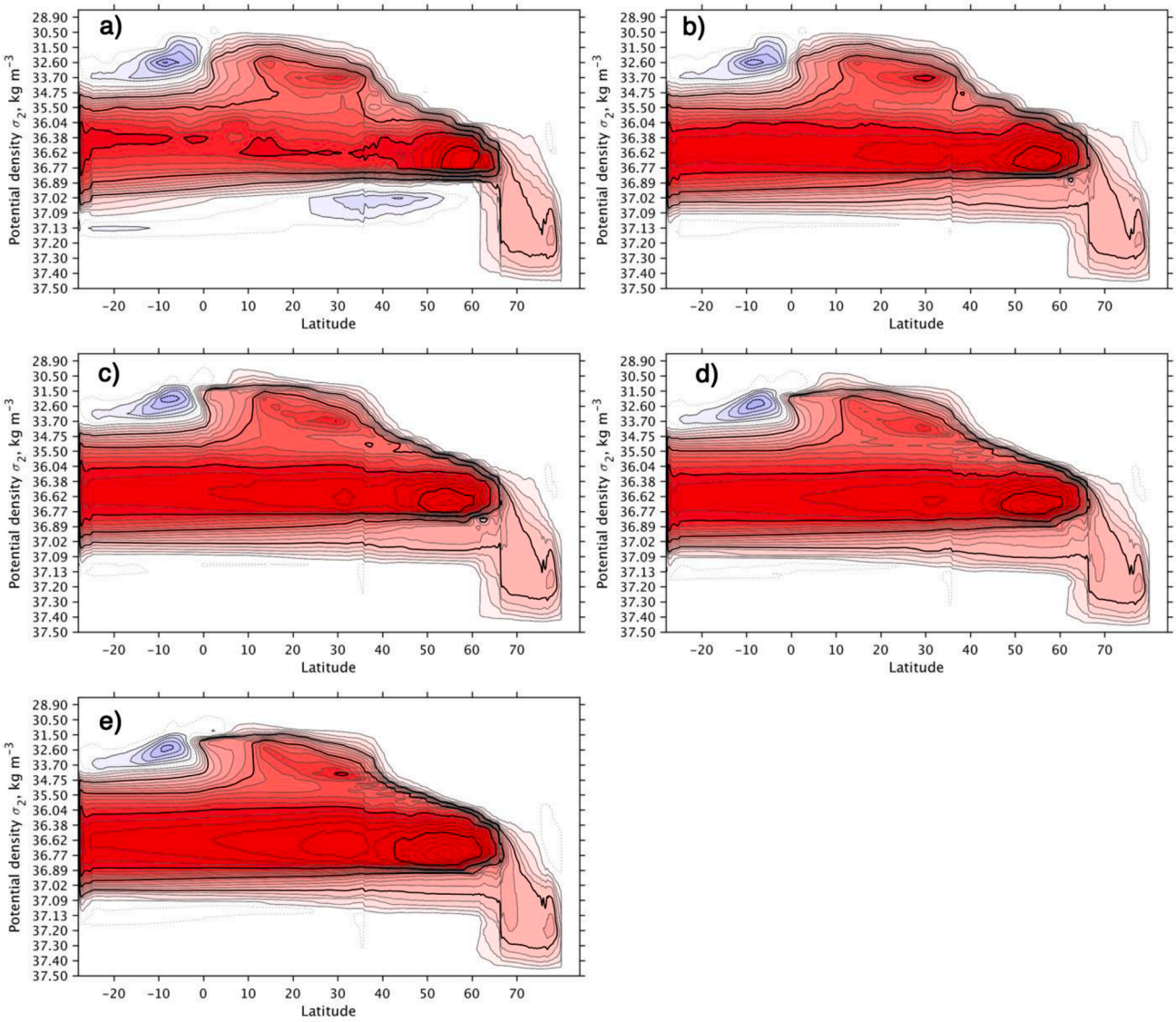

Fig. 15. Modeled time mean meridional overturning streamfunction (in Sv) as a function of density (σ_2, kg/m^3) and latitude in five 1/12° Atlantic HYCOM simulations with different vertical resolutions: (a) 16, (b) 24, (c) 32, (d) 64, and (e) 96 layers, respectively. The results show that expect the 16-layer simulation, the other four simulations have an overall similar overturning streamfunction structure.

increases, the modeled southward NADW component becomes deeper and much closer to the observations. This highlights that increased vertical resolution leads to a better representation of the water masses comprising the AMOC (e.g., NADW).

The AMOC is also evaluated in streamfunction with respect to density ψ_σ, which is defined as the integrated meridional transport (Sv) across the basin above a constant density surface. The ψ_σ connects directly to water mass transformation (Xu et al., 2018) and is more useful in describing the AMOC in the high latitude where the northward and southward components, along the eastern and western side of the basin, respectively, takes place at a similar depth, but on different density surface (due to the sloping isopycnic surface across the basin in the northern latitudes). Fig. 15 shows the streamfunction ψ_σ from these simulations. The picture is similar to that in Fig. 12, in that the four higher resolution simulations show a qualitatively consistent structure of overturning streamfunction, including both the basin-scale AMOC, and smaller sub-basin scale overturning in the subtropical (centered near 30°N and 34 kg/m^3) and subpolar (centered near 55°N and 36.77 kg/m^3). The latter represents the diapycnal transformation associated with the subtropical/subpolar gyres; see Xu et al. (2016; 2018) for more discussions. As for ψ_z streamfunctions, the 16-layer simulation exhibits a somewhat similar structure to the higher vertical resolution simulations in the northward-flowing part of the streamfunction, but the overturning strength is much weaker and the southward component does not have any overflow water contribution south of the 65°N. This indicates that, due to lack of vertical resolution, the modeled overflow water in not well represented with thick shallow layers and becomes part of LSW after spilling over the sill. The overflow water masses underwent a significant density change from its source to final product water downstream (e.g., Legg et al., 2009), and the vertical resolution in the 16-layer configuration is too coarse for that transformation. A similar deficiency can be found in a regional modeling of the Mediterranean outflow when vertical resolution is too coarse (Xu et al., 2007).

As in Figs. 14, 16 displays the difference in overturning streamfunction, but in density coordinate. Here the results also show a lower streamfunction value in the coarser vertical resolution (16- to 64-layer) simulations and the difference is mostly centered near the LSW density range (i.e., the blue patch centered in near 36.77–36.89 kg/m^3). The magnitude of difference as defined in density coordinate, from more than 12 Sv in 16-layer to 6 Sv in 64-layer, is about 2 times of that in z-

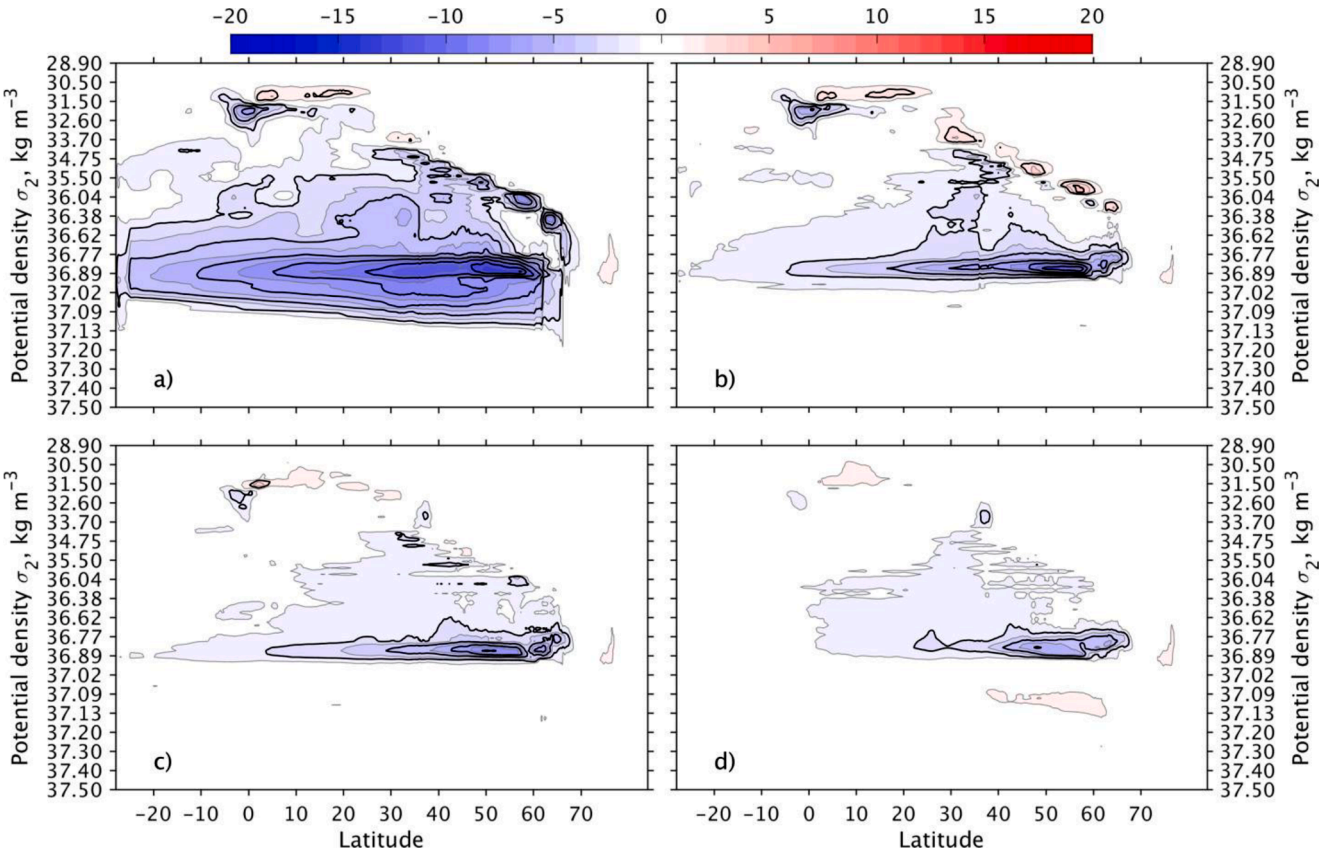

Fig. 16. Difference in modeled time-mean meridional overturning streamfunction (in Sv) as a function of density and latitude in four 1/12 Atlantic HYCOM simulations with a) 16, (b) 24, (c) 32, and (d) 64 layers, respectively, compared to the 96-layer simulation as a reference. Blue color indicates streamfunction value is lower in the low-resolution simulation and vice versa. The gray and black contours are with 1 and 2 Sv interval, respectively.

coordinate. It should be emphasized that the differences in Fig. 16 in streamfunctions is not so much about a stronger or weaker overturning, but more about the overturning streamfunctions on a slightly lighter/denser density.

Like the RAPID observations in the subtropical region, the OSNAP observations (Lozier et al., 2019) provided a benchmark to quantitatively evaluate the modeled AMOC structure in the subpolar North Atlantic, where the NADW is formed. Fig. 17 compares the density structure of the AMOC for both the western section from Labrador to Greenland, eastern section from Greenland to Scotland, and combined full sections (see Fig. A1 in the appendix for locations). When the OSNAP section is considered as a whole, all model simulations produce stronger overturning than observed, with more LSW and similar transport of overflow water (Fig. 17a). The stronger overturning is attributed mostly to a stronger overturning across the western section as the overturning across the eastern section is comparable between model and observations (Figs. 17b-c). When the model sensitivity is considered, the four simulations (24- to 96-layer) show a similar transformation structure, whereas the 16-layer simulation lacks a contribution from the dense overflow water (Fig. 17b).

3.3. *Horizontal structure of the subtropical and subpolar North Atlantic circulation*

The AMOC, as discussed in previous section, provides a zonally integrated view of the basin-wide circulation in the North Atlantic. For a comprehensive view, one should also examine the horizontal structure of the circulation. Fig. 18 displays the modeled cumulative transport (from west to east) along the RAPID line near 26°N for the upper and lower limb of the AMOC, separated by density (σ_2) interface of 36.52 kg/m^3 which is located at approximately 1000 m and slightly shallower on the western side (Fig. 18b). Above this interface, one can see the signature of the northward western boundary current transports in the Florida Strait and east of Abaco (i.e., the Florida Current and Antilles Current, respectively), and the broad southward transport over the Atlantic basin east of about 70°W. The latter is comparable to the Sverdrup transport that is calculated from the wind stress curl (dashed black line in Fig. 18a). This is not surprising as the interior flow of the subtropical North Atlantic gyre is, to a good approximation, in Sverdrup balance (Wunsch and Roemmich, 1985; Schmitz et al., 1992; Wunsch, 2011). In the lower limb, the modeled circulation pattern across this latitude consists of a southward DWBC and some recirculation west of 70°W. East of 70°W in the ocean interior, the cumulative time-mean transport is relatively flat (Fig. 18a), indicating that there is no significant meridional mean flow across this latitude in the model. Overall, all five experiments exhibit a similar transport pattern (Fig. 18), except again for the 16-layer case. Thus, the vertical resolution does not play a significant role in defining the horizontal structure of the meridional transports in the subtropical North Atlantic for 32+ layers.

A similar plot can be performed further north for the subpolar region. Fig. 19 displays the eastward cumulation of the meridional transport in the upper and lower limbs of the AMOC across the northern North Atlantic along the east OSNAP section from Greenland to Scotland near 59°N. The upper and lower limbs are separated by the density surface σ_2= 36.6 kg/m^3 (equivalent to σ_θ of 27.50 kg/m^3) as shown in Fig. 19b. In the upper limb, both the magnitude and structure of the modeled transport are comparable to the observations. In the lower limb, the transport structure agrees, but the magnitude of the modeled transport is significantly higher than in the OSNAP observations. The largest difference is found in the Irminger Basin. The modeled full water column western boundary current transport is about 40 Sv (Fig. 20), compared to 31.2 Sv in OSNAP observations during 2014–2018. The historical

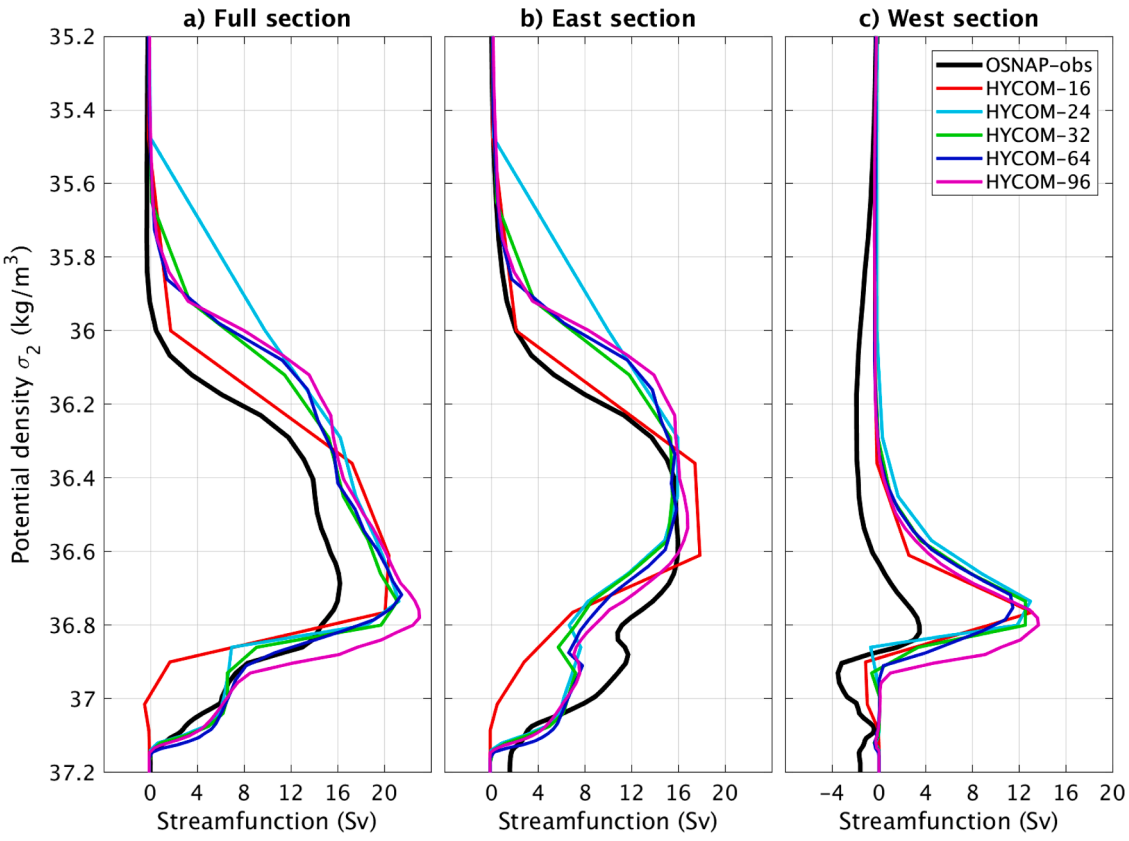

Fig. 17. Time mean meridional overturning streamfunction (in Sv) across the OSNAP sections from the observations and five 1/12° Atlantic HYCOM simulations with different vertical resolutions from 16 to 96 layers. The results are presented for (a) full section (Labrador-Greenland-Scotland), (b) East section (Greenland-Scotland), and west section (Labrador-Greenland).

observations of the western boundary current at this location have yielded a similar volume transport of 32.1 Sv (Sarafanov et al., 2012) and 33.1 Sv (Daniault et al., 2016), from 7 annual surveys in 2002–2008 and 6 biannual surveys in 2002–2012, respectively. The higher model transport is associated with a stronger gyre recirculation in the LSW layer. As in the subtropics, the horizontal circulation does not differ much with 32 or more layers.

East of about 39°W across the east OSNAP section, the modeled full water column meridional flow is generally northward, including contributions of both the subpolar gyre and the AMOC components. Interestingly, the pattern of the modeled full water column transport between 39°W and eastern boundary is comparable to that of the Sverdrup transport (Fig. 20 dashed line), even though the agreement is not as good as in the subtropics. The deviations are found in the 30–20°W range where the subpolar gyre recirculates around the Iceland Basin, including a standing eddy centered near 22°W in the deepest portion of the Iceland Basin (Fig. 20b). The agreement between the modeled transport and the Sverdrup transport is surprising because a) the Sverdrup balance is not deemed to hold at this latitude where it takes multiple decades to achieve dynamical equilibrium (Wunsch, 2011) and b) the AMOC is deemed as driven by basin-scale density difference, not by the wind within the subpolar North Atlantic. The results in Fig. 20 suggest that much of the modeled subpolar circulation is driven by the large-scale wind, although the water masses undergo buoyancy loss and become denser as they flow around the northern rim of the subpolar North Atlantic. Regarding to model sensitivity, other than a weaker recirculation in the Iceland Basin in the 16-layer simulation, all five simulations exhibit similar zonal structure of the full-water column transport across this section. Thus, except for the 16-layer configuration, the vertical resolution does not play a significant role in the horizontal structure of the barotropic transports in the subpolar North Atlantic.

4. Summary and discussion

As pointed out in Stewart et al. (2017), few studies have documented the impact of the vertical resolution on OGCMs and there is no consensus on how one should construct the vertical grid to represent the vertical structure of the baroclinic modes as well as the distribution of distinct water masses throughout the global ocean. Stewart et al. (2017) proposed that the purpose of a vertical grid is primarily to resolve the vertical structure of the horizontal flow and that the vertical grids should be constructed based on their ability to represent baroclinic modal structure. Although not emphasized in Stewart et al. (2017), another fundamental purpose of the vertical grids in OGCMs is to represent accurately the distinct water masses that originate in different part of the ocean and occupy/circulate in different depth and/or density range of the water column. This study examines the impact of vertical resolution on a) the baroclinic modes and b) water mass representation and the large-scale circulation in the Atlantic. We find that both the 50 well-positioned z levels of Stewart et al. (2017) and the standard 32-layer HYCOM configuration are adequate to represent the zero-crossing depths of the first five baroclinic modes in mid-latitudes. The current OGCMs horizontal resolution resolves at most the first five Rossby radii of deformation and the vertical resolution currently used in OGCMs is therefore adequate in representing the corresponding vertical structure of the first five modes. The most commonly used OGCM vertical grids also satisfy the vertical grid requirement of Stewart et al. (2017) for the first two modes, but there is a definitely an advantage in using density layers instead of levels in representing higher modes. A 100-level geopotential configuration cannot satisfy fully Stewart et al. (2017)'s grid requirement for the first five modes while a 96-layer isopycnic configuration does. This is primarily because a minimum of three levels is required in z-coordinate model to represent a

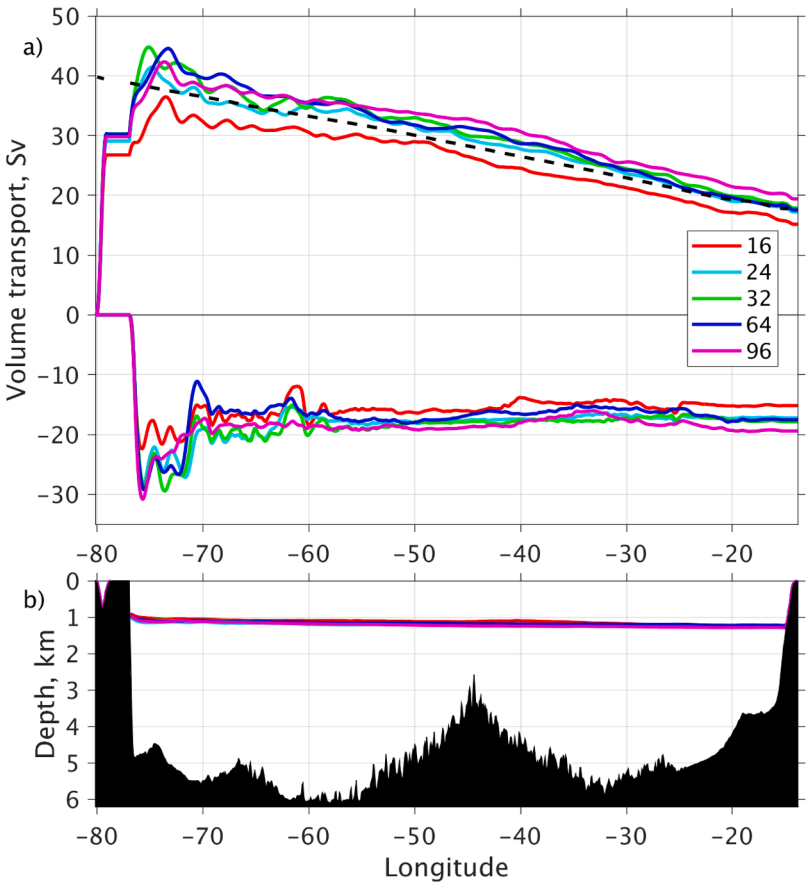

Fig. 18. Horizontal structure of the subtropical circulation along the RAPID line near 26°N. a) Time-mean (eastward) cumulative volume transport (in Sv) in the upper and lower limbs of the Atlantic meridional overturning circulation (AMOC) from five 1/12° HYCOM simulations, with vertical resolution of 16, 24, 32, 64, and 96 layers, respectively. The black dash line indicates the Sverdrup transport calculated from wind-stress curl, integrated westward and multiplied by −1 to be comparable with the eastward cumulative upper limb transports; (b) bathymetry along the RAPID line and the interface of density surface that separates the upper (northward) and lower (southward) limb of the AMOC.

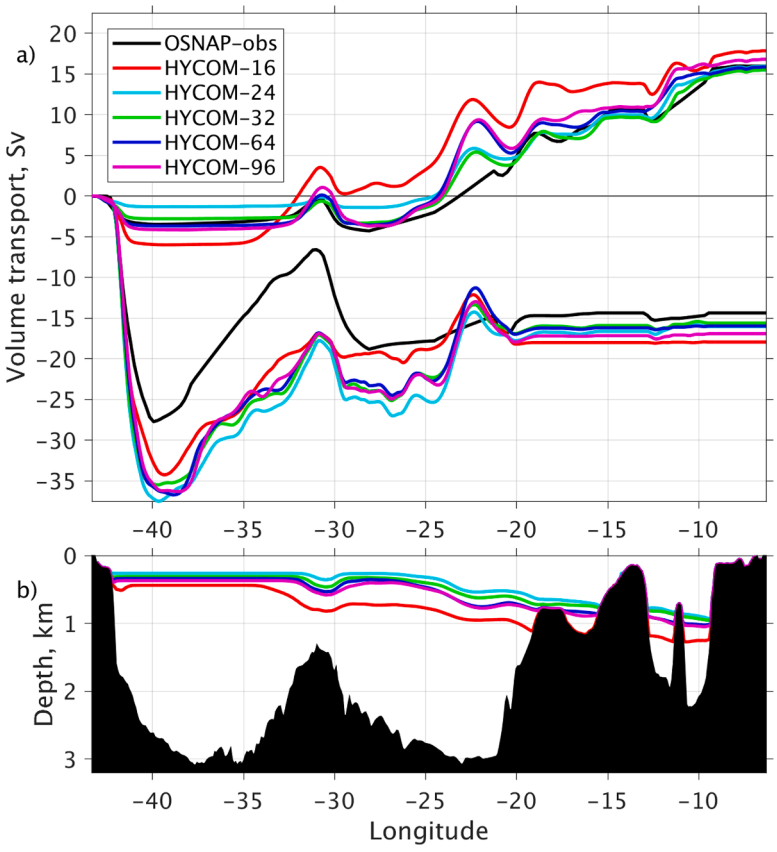

Fig. 19. Horizontal structure of the subpolar circulation along the east OSNAP section from Greenland to Scotland (see Fig. A1 for location). a) Time-mean (eastward) cumulative volume transport (in Sv) in the upper and lower limbs of the Atlantic meridional overturning circulation (AMOC) from five 1/12° HYCOM simulations, with vertical resolution of 16, 24, 32, 64, and 96 layers, respectively; black line denote the observational estimate from b) bathymetry along the RAPID line and the interface of density surface of 27.50 kg/m^3 that separates the upper (northward) and lower (southward) limb of the AMOC.

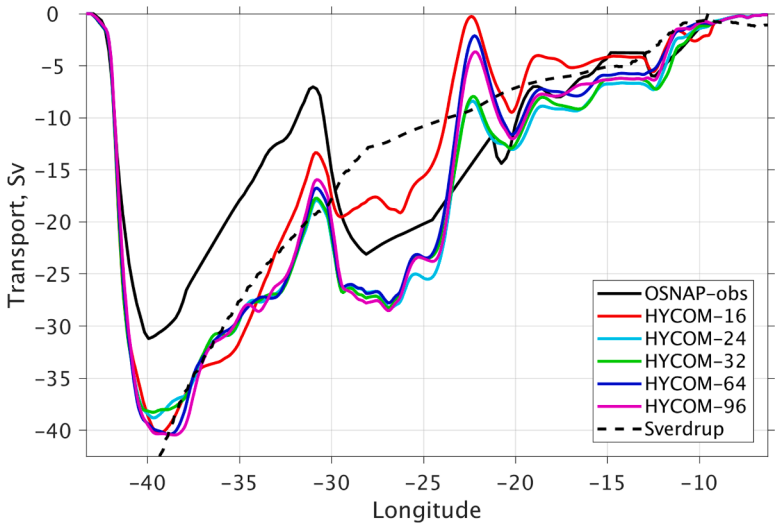

Fig. 20. Cumulative (eastward) full water column transport along the east ONSAP section. Solid black line is estimated from OSNAP observations; colored lines are the model transports from five 1/12° HYCOM simulations, with vertical resolution of 16, 24, 32, 64, and 96 layers, respectively; black dashed line are the Sverdrup transport calculated from wind stress curl.

single water mass versus only one constant density layer in isopycnic coordinate models, thus giving a factor of three advantage to the latter.

Vertical resolution significantly impacts the representation of deep water masses and hence the structure of the Atlantic meridional overturning circulation (AMOC). A coarse vertical resolution (16 layers) simulation exhibits virtually no transport in the dense overflow water which leads to a weaker and significantly shallower AMOC despite resolving the first baroclinic mode throughout the domain, whereas there are overall very small differences in the subtropical and subpolar North Atlantic circulation in the simulations with finer vertical resolution (24 to 96 layers). As the vertical resolution is increased from 24 to 96 layers, there is a slight increase in the magnitude of the AMOC and a slight deepening of the southward-flowing North Atlantic Deep Water that leads to a better agreement with the observations.

With increased vertical resolution, the OGCMs better resolve both the vertical modes and the water masses, but their relative importance differs. With 16 layers, the vertical resolution can represent the first baroclinic Rossby radius and the vertical structure of the first baroclinic mode to a good approximation. It however cannot represent the dense overflow water which leads to a rather unrealistic structure of the AMOC. The lower SSH variability seen in the 16-layer configuration primarily viewed as a consequence of not resolving higher baroclinic modes, but the weaker AMOC may also lead to a weaker and less unstable northward-flowing Gulf Stream and North Atlantic Current.

In conclusion, we argue that accurately representing the water mass is more important than representing the vertical modes in simulating the basin-scale circulation and mesoscale variability and should be considered first when constructing a vertical grid. This does not mean that the vertical modes are not important and, with higher horizontal resolution that now starts to resolve sub-mesoscale eddies, one could see more sensitivity to vertical resolution, especially at higher frequencies and in the presence of internal tides (Xu et al., 2022). High vertical resolution is expected to be beneficial in the representation of the stratification associated with the pycnocline, hence the generation of internal tides. Also, in this study we have focused on whether or to what extent the vertical resolution impacts the basin-scale aspects of the North Atlantic circulation (i.e., AMOC and subpolar/subtropical gyres). Vertical resolution can also impact regional processes, such as upwelling and associated diapycnal mixing. The impact on these detailed processes needs to be further examined in future studies.

CRediT authorship contribution statement

Xiaobiao Xu: Conceptualization, Methodology, Writing – original draft. **Eric P. Chassignet:** Methodology, Supervision, Writing – review & editing. **Alan J. Wallcraft:** Methodology.

Declaration of Competing Interest

The authors declare that they have no known competing financial interests or personal relationships that could have appeared to influence the work reported in this paper.

Data availability

The Mean Dynamic topography (MDT) are available in AVISO (https://aviso.altimetry.fr); the gridded Sea Surface Height (SSH) are distributed through Copernicus Marine Service (https://marine.copernicus.eu); the RAPID observations are available at https://rapid.ac.uk; and the OSNAP observations are available at https://o-snap.org. The full-resolution model outputs are stored in the U.S. Army Engineer Research and Development Center (ERDC) and U.S. Navy DoD Supercomputing Resource Center (DSRC) archive server. The key model results represented in this study are available in the data repository (http://doi.org/10.5281/zenodo.7751007). The script to run the numerical simulations and to plot the figures presented in the paper are available by request.

Acknowledgment

XX, EPC, and AJW acknowledge support from the Office of Naval Research (ONR) grants N00014–19–1-2717 and N00014–20–1-2769, the National Science Foundation's Directorate of Geosciences and the National Environment Research Council of the United Kingdom (NSFGEO-NERC) award 2038449, and the National Aeronautics and Space Administration (NASA) grants 80NSSC20K1135 and 80NSSC21K1500. The high-resolution HYCOM simulations were performed on supercomputers at the U.S. Army Engineer Research and Development Center (ERDC) in Vicksburg, Mississippi, and the U.S. Navy DoD Supercomputing Resource Center (DSRC) in Stennis Space Center, Mississippi, using computer time provided by the U.S. DoD High Performance Computing Modernization Program. The authors also

thank Dr. Stewart and the anonymous reviewer for their constructure comments, which improves this paper significantly.

Appendix

(a) Depth and layer distribution of the first 9 baroclinic modes

The zero-crossing interfaces of baroclinic mode divide the water column in layers. For example, the first baroclinic mode has one zero-crossing interface which divides the water column into two layers, the second baroclinic mode has two zero-crossing interfaces that divide the water column into three layers, etc. Table A1 lists the spatially averaged depth of the zero-crossing interfaces associated with the baroclinic modes 1, 2, 3, 5, 7, and 9. These z levels can be used to construct the low-resolution configuration to represent the Rossby radius (and/or vertical modes) in z-level coordinate (Figs. 2a–c, 3a–c). Table A2 lists the spatially averaged densities of the layers that are divided by these zero-crossing interfaces and can be used to construct the low-resolution configuration to represent the Rossby radius (and/or vertical modes) in isopycnic coordinate (Figs. 2d–f, 3d–f).

Table A1
Spatially averaged depth (in meter) of the zero-crossing interfaces of the baroclinic modes 1, 2, 3, 5, 7, and 9 in the North and Equatorial Atlantic Ocean as calculated from ocean climatology GDEM.

Interface index	$m = 1$	$m = 2$	$m = 3$	$m = 5$	$m = 7$	$m = 9$
1	1170	286	132	63	48	41
2		1787	694	292	172	124
3			2136	693	397	272
4				1271	691	466
5				2557	1068	698
6					1620	979
7					2779	1329
8						1876
9						2915

Table A2
Spatially averaged densities (σ_2 in kg/m^3) of the layers divided by the zero-crossing interface of the baroclinic modes 1, 2, 3, 5, and 9 in the North and Equatorial Atlantic Ocean as calculated from ocean climatology GDEM.

Layer index	$m = 1$	$m = 2$	$m = 3$	$m = 5$	$m = 7$	$m = 9$
1	35.80	34.45	33.80	33.46	33.37	33.33
2	36.96	36.42	35.65	34.91	34.42	34.12
3		37.01	36.71	35.88	35.41	35.08
4			37.03	36.50	35.98	35.63
5				36.90	36.41	36.05
6				37.04	36.73	36.37
7					36.95	36.63
8					37.05	36.83
9						36.98
10						37.05

(b) North and Equatorial Atlantic HYCOM configuration

The North and Equatorial Atlantic HYCOM computational domain extends from 28°S to the Fram Strait at 80°N (Fig. A1). The northern and southern boundaries are "vertical wall" with no normal flows, and within a buffer zone of 3° to these two boundaries, the model temperature and salinity are restored to monthly ocean climatology (Carnes 2009) with an *e*-folding time of 5–60 days, which increases with distance from the boundary. The atmospheric forcing combines the climatological monthly means from the 40-year European Center for Medium Range Weather Forecasts Reanalysis (ERA040, Uppala et al., 2005) and high-frequency (6-hourly) wind anomalies from the Fleet Numerical Meteorology and Oceanography Center's Navy Operational Global Atmospheric Prediction System (NOGAPS, Rosmond et al., 2002). The reason for the latter is that ocean convection is strongly influenced by synoptic weather systems and high-frequency winds are important for proper representation of the surface mixed layer physics (Kantha and Clayson, 1994; Large et al., 1994). Wind anomalies for year 2003, a year with neutral North Atlantic Oscillation is used for this purpose. The surface heat flux includes the shortwave and longwave radiations that are directly from ERA-40, and the latent and sensible heat fluxes that are calculated using the model sea surface temperature (SST) and bulk formulas of Kara et al. (2005). The surface freshwater flux includes evaporation, precipitation, and river runoffs. The model sea surface salinity is also restored toward the monthly climatology with a relatively strong restoring strength of 15 m per 30 days.

Five simulations are considered in this study, all with an eddying horizontal resolution of 1/12° and a vertical resolution of 16, 24, 32, 64, and 96 layers, respectively. The 32-layer configuration was the standard of the Atlantic simulation (Xu et al., 2010; 2012), from which the resolution is doubled and tripled in the 64 and 96-layer configurations (by inserting one and two model layers between each two layers) and cut in half in the 16-layer configuration (combining two layers into one). The 24-layer configuration was designed to investigate the impact of reducing resolution in the upper water column (the top 8 model layers are the same as in the 16-layer configuration and the lower 16 layers are the same as the standard 32-layer configuration).

All five simulations are initialized with January temperature and salinity from ocean climatology (Carnes 2009) and run for 20 years. Fig. A2

displays a vertical view of the model layers in the initialization along the RAPID section near 26°N, for 16, 32, and 96-layer configurations, from which one can see that the resolution below about 1500 m is quite coarse in the 16-layer set up. We focus on the last five years of the integration, which is deemed to be representative of the circulation after spin-up, i.e., the simulation reaches statistical equilibrium in terms of kinetic energy and volume transports, although the modeled temperature and salinity are expected to continue to adjust over much longer time scales.

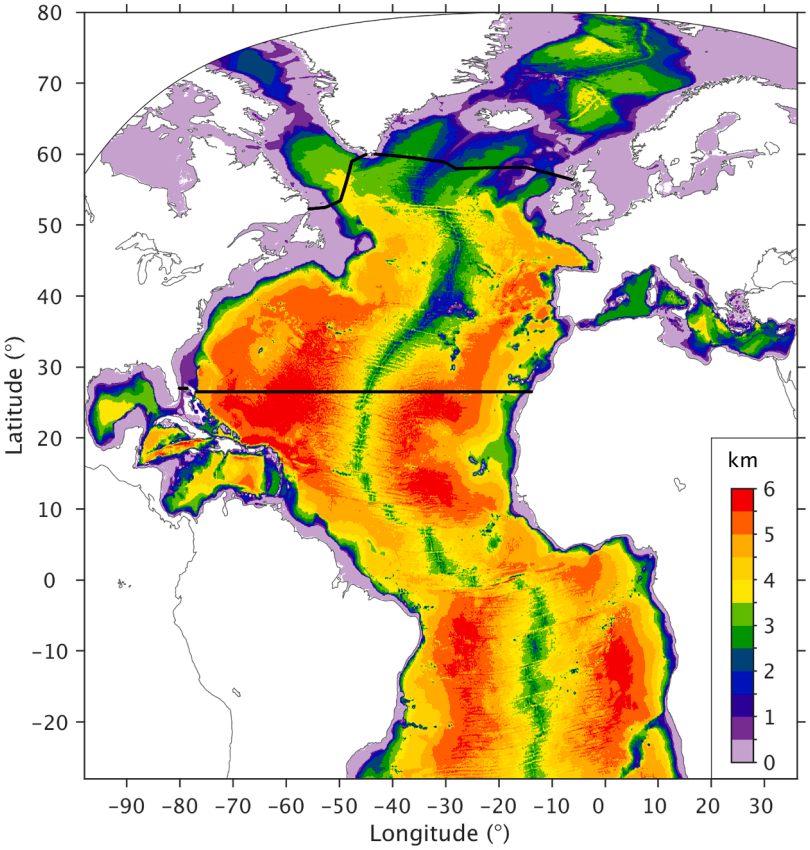

Fig. A1. Bathymetry (in km) of the North and equatorial Atlantic domain used in the HYCOM simulations with different vertical resolutions. Black lines near 26°N and across the subpolar region denote the location of the RAPID (e.g., Smeed et al., 2018) and the OSNAP (e.g., Loizer et al., 2019) observations, to which the modeled transport structure is examined in detail.

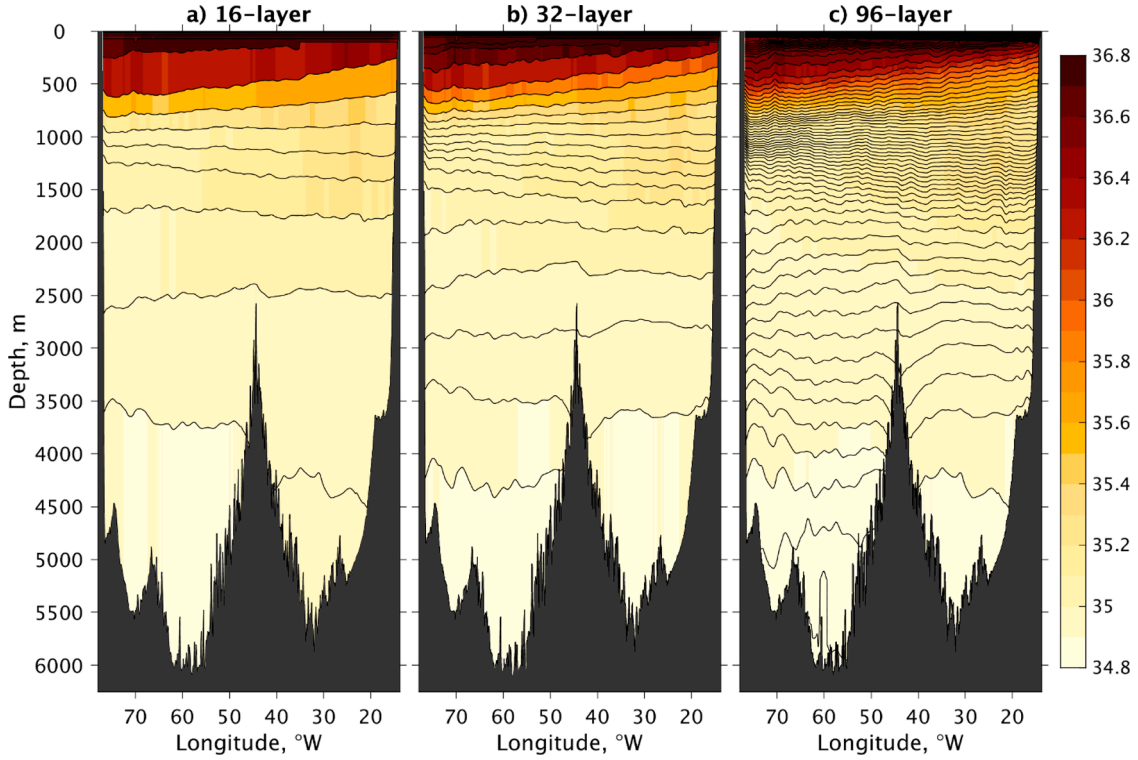

Fig. A2. Model initial salinity along with the model layer interfaces across the Atlantic along the RAPID line in three 1/12° HYCOM simulations with different 16, 32, and 96 layers, respectively.

References

Adamec, D., 1988. Numerical simulations of the effects of seamounts and vertical resolution on strong ocean flows. J. Phys. Oceanogr. 18, 258–269.

Ajayi, A., Le Sommer, J., Chassignet, E.P., Molines, J.M., Xu, X., Albert, A., Cosme, E., 2020. Spatial and temporal variability of North Atlantic eddy field from two kilometric-resolution ocean models. J. Geophys. Res.-Oceans 125 (5), e2019JC015827.

Ajayi, A., Le Sommer, J., Chassignet, E.P., Molines, J.-M., Xu, X., Albert, A., Dewar, W., 2021. Diagnosing cross-scale kinetic energy exchanges from two submesoscale permitting ocean models. J. Adv. Model. Earth Syst. 13 (6), e2019MS001923.

Barnier, B., Hua, B.L., Provost, C.L., 1991. On the catalytic role of high baroclinic modes in eddy-driven large-scale circulations. J. Phys. Oceanogr. 21, 976–997.

Bleck, R., 2002. An oceanic general circulation model framed in hybrid isopycnic-Cartesian coordinates. Ocean Model. 4, 55–88.

Bryan, K., 1969. A numerical method for the study of the circulation of the world ocean. J. Comput. Phys. 4, 347–376.

Carnes, M.R., 2009. Description and Evaluation of GDEM-V3.0. Naval Research Laboratory Memo, p. 21. Rep. NRL/MR/7330–09-9165Available online at. http://www7320.nrlssc.navy.mil/pubs/2009/carnes-2009.pdf.

Chassignet, E.P., Xu, X., 2017. Impact of horizontal resolution (1/12° to 1/50°) on Gulf Stream separation, penetration, and variability. J. Phys. Oceanogr. 47, 1999–2021.

Chassignet, E.P., Xu, X., 2021. On the importance of high-resolution in large scale ocean models. Adv. Atmos. Sci. 38, 1621–1634.

Chassignet, E.P., Smith, L.T., Halliwell, G.R., Bleck, R., 2003. North Atlantic simulations with the hybrid coordinate ocean model (HYCOM): impact of the vertical coordinate choice, reference pressure, and thermobaricity. J. Phys. Oceanogr. 33, 2504–2526.

Chassignet, E.P., Hurlburt, H.E., Smedstad, O.M., Halliwell, G.R., Wallcraft, A.J., Metzger, E.J., Blanton, B.O., Lozano, C., Rao, D.B., Hogan, P.J., Srinivasan, A., 2006. Generalized vertical coordinates for eddy-resolving global and coastal ocean forecasts. Oceanography 19, 20–31.

Chassignet, E.P., Yeager, S.G., Fox-Kemper, B., Bozec, A., Castruccio, F., Danabasoglu, G., Horvat, C., Kim, W.M., Koldunov, N., Li, Y., Lin, P., Liu, H., Sein, D., Sidorenko, D., Wang, Q., Xu, X., 2020. Impact of horizontal resolution on global ocean-sea-ice model simulations based on the experimental protocols of the ocean model intercomparison project phase 2 (OMIP-2). Geosci. Model Dev. 13, 4595–4637.

Chassignet, E.P., Xu, X., Bozec, A., Uchida, T., 2023. Impact of the New England seamount chain on Gulf Stream pathway and variability. J. Phys. Oceanogr. 53 (8), 1871–1886.

Chelton, D.B., DeSzoeke, R.A., Schlax, M.G., El Naggar, K., Siwertz, N., 1998. Geographical variability of the first baroclinic Rossby radius of deformation. J. Phys. Oceanogr. 28 (3), 433–460.

Daniault, N., Mercier, H., Lherminier, P., Sarafanov, A., Falina, A., Zunino, P., Pérez, F.F., Ríos, A.F., Ferron, B., Huck, T., Thierry, V., 2016. The northern North Atlantic ocean mean circulation in the early 21st century. Prog. Oceanogr. 146, 142–158.

Frajka-Williams, E., Ansorge, I.J., Baehr, J., Bryden, H.L., Chidichimo, M.P., Cunningham, S.A., Danabasoglu, G., Dong, S., Donohue, K.A., Elipot, S., 2019. Atlantic meridional overturning circulation: observed transport and variability. Front. Mar. Sci. 6, 260.

Hallberg, R., 2013. Using a resolution function to regulate parameterizations of oceanic mesoscale eddy effects. Ocean Model. 72, 92–103.

Hirschi, J.J.M., Barnier, B., Böning, C., Biastoch, A., Blaker, A.T., Coward, A., Danilov, S., Drijfhout, S., Getzlaff, K., Griffies, S.M., Hasumi, H., Hewitt, H., Iovino, D., Kawasaki, T., Kiss, A.E., Koldunov, N., Marzocchi, A., Mecking, J.V., Moat, B., Molines, J.M., Myers, P.G., Penduff, T., Roberts, M., Treguier, A.M., Sein, D.V., Sidorenko, D., Small, J., Spence, P., Thompson, L., Weijer, W., Xu, X., 2020. The Atlantic meridional overturning circulation in high-resolution models. J. Geophys. Res. Oceans 125, e2019JC015522.

Hurlburt, H.E., Hogan, P.J., 2000. Impact of 1/8° to 1/64° resolution on Gulf Stream model–data comparisons in basin-scale subtropical Atlantic Ocean models. Dyn. Atmos. Oceans 32, 283–329.

Kantha, L.H., Clayson, C.A., 1994. An improved mixed layer model for geophysical applications. J. Geophys. Res. Oceans 99, 25235–25266.

Kara, A.B., Hurlburt, H.E., Wallcraft, A.J., 2005. Stability dependent exchange coefficients for air–sea fluxes. J. Atmos. Oceanic Technol. 22, 1080–1094.

Klein, P., Lapeyre, G., Siegelman, L., Qiu, B., Fu, L.L., Torres, H., Su, Z., Menemenlis, D., Le Gentil, S., 2019. Ocean-scale interactions from space. Earth Space Sci. 6, 795–817.

Lévy, M., Klein, P., Tréguier, A.M., Iovino, D., Madec, G., Masson, S., Takahashi, K., 2010. Modifications of gyre circulation by sub-mesoscale physics. Ocean Model. 34, 1–15.

Large, W.G., McWilliams, J.C., Doney, S.C., 1994. Ocean vertical mixing: a review and a model with a nonlocal boundary layer parameterization. Rev. Geophys. 32, 363–403.

Le Sommer, J., Chassignet, E.P., Wallcraft, A.J., Chassignet, E., Pascual, A., Tintoré, J., Verron, J., 2018. Ocean circulation modeling for operational oceanography: current status and future challenges. New Frontiers in Operational Oceanography. GODAE OceanView, pp. 289–306.

Legg, S., Chang, Y., Chassignet, E.P., Danabasoglu, G., Ezer, T., Gordon, A.L., Griffes, S., Hallberg, R., Jackson, L., Large, W., Özgökmen, T., Peters, H., Price, J., Riemenschneider, U., Wu, W., Xu, X., Yang, J., 2009. Improving oceanic overflow representation in climate models: the gravity current entrainment climate process team. Bull. Amer. Met. Soc. 90, 657–670.

Lozier, M.S., Li, F., Bacon, S., Bahr, F., Bower, A.S., Cunningham, S.A., de Jong, M.F., de Steur, L., deYoung, B., Fischer, J., Gary, S.F., 2019. A sea change in our view of overturning in the subpolar. North Atlantic. Sci. 363 (6426), 516–521.

McWilliams, J.C., 1996. Modeling the oceanic general circulation. Annu. Rev. Fluid Mech. 28, 215–248.
Mulet, S., Rio, M.H., Etienne, H., Artana, C., Cancet, M., Dibarboure, G., Feng, H., Husson, R., Picot, N., Provost, C., Strub, P.T., 2021. The new CNES-CLS18 global mean dynamic topography. Ocean Sci. 17, 789–808.
Paiva, A.M., Hargrove, J.T., Chassignet, E.P., Bleck, R., 1999. Turbulent behavior of a fine mesh (1/12 degree) numerical simulation of the North Atlantic. J. Mar. Syst. 21, 307–320.
Richardson, P.L., 1983. Eddy kinetic energy in the North Atlantic from surface drifters. J. Geophys. Res. 88, 4355–4436.
Roberts, M.J., Jackson, L.C., Roberts, C.D., Meccia, V., Docquier, D., Koenigk, T., Ortega, P., Moreno-Chamarro, E., Bellucci, A., Coward, A., Drijfhout, S., Exarchou, E., Gutjahr, O., Hewitt, H., Iovino, D., Lohmann, K., Schiemann, R., Seddon, J., Terray, L., Xu, X., Zhang, Q., Chang, P., Yeager, S.G., Castruccio, F.S., Zhang, S., Wu, L., 2020. Sensitivity of the Atlantic meridional overturning circulation to model resolution in CMIP6 HighResMIP simulations and implications for future changes. J. Adv. Model. Earth Syst. 12, e2019MS002014.
Rosmond, T., Teixeira, J., Peng, M., Hogan, T., Pauley, R., 2002. Navy operational global atmospheric prediction system (NOGAPS): forcing for ocean models. Oceanogr 15, 99–108.
Sarafanov, A., Falina, A., Mercier, H., Sokov, A., Lherminier, P., Gourcuff, C., Gladyshev, S., Gaillard, F., Daniault, N., 2012. Mean full-depth summer circulation and transports at the northern periphery of the Atlantic ocean in the 2000s. J. Geophys. Res.Oceans. 117, C01014.
Schmitz, W.J., Thompson, J.D., Luyten, J.R., 1992. The Sverdrup circulation for the Atlantic along 24°N. J. Geophys. Res. Oceans 97, 7251–7256.
Smeed, D.A., Josey, S.A., Beaulieu, C., Johns, W.E., Moat, B.I., Frajka-Williams, E., Rayner, D., Meinen, C.S., Baringer, M.O., Bryden, H.L., McCarthy, G.D., 2018. The North Atlantic ocean is in a state of reduced overturning. Geophys. Res. Lett. 45, 1527–1533.
Smith, L.T., Chassignet, E.P., Bleck, R., 2000. The impact of lateral boundary conditions and horizontal resolution on North Atlantic water mass transformations and pathways in an isopycnic coordinate ocean model. J. Phys. Oceanogr. 30, 137–159.
Soufflet, Y., Marchesiello, P., Lemarié, F., Jouanno, J., Capet, X., Debreu, L., Benshila, R., 2016. On effective resolution in ocean models. Ocean Model. 98, 36–50.
Stanley, G.J., 2019. Neutral surface topology. Ocean Model. 138, 88–106.
Stewart, K.D., Hogg, A.M., Griffies, S.M., Heerdegen, A.P., Ward, M.L., Spence, P., England, M.H., 2017. Vertical resolution of baroclinic modes in global ocean models. Ocean Model. 113, 50–65.
Uchida, T., Le Sommer, J., Stern, C., Abernathey, R.P., Holdgraf, C., Albert, A., Brodeau, L., Chassignet, E.P., Xu, X., Gula, J., Roullet, G., Koldunov, N., Danilov, S., Wang, Q., Menemenlis, D., Bricaud, C., Arbic, B.K., Shriver, J.F., Qiao, F., Xiao, B., Biastoch, A., Schubert, R., Fox-Kemper, B., Dewar, W.K., 2022. Cloud-based framework for inter-comparing submesoscale permitting realistic ocean models. Geosci. Model Dev. 15 (14), 5829–5856.
Uppala, S.M., KÅllberg, P.W., Simmons, A.J., Andrae, U., Da Costa Bechtold, V., Fiorino, M., Gibson, J.K., Haseler, J., Hernandez, A., Kelly, G.A., Li, X., Onogi, K., Saarinen, S., Sokka, N., Allan, R.P., Andersson, E., Arpe, K., Balmaseda, M.A., Beljaars, A.C.M., Van De Berg, L., Bidlot, J., Bormann, N., Caires, S., Chevallier, F., Dethof, A., Dragosavac, M., Fisher, M., Fuentes, M., Hagemann, S., Hólm, E., Hoskins, B.J., Isaksen, L., Janssen, P.A.E.M., Jenne, R., Mcnally, A.P., Mahfouf, J.F., Morcrette, J.J., Rayner, N.A., Saunders, R.W., Simon, P., Sterl, A., Trenberth, K.E., Untch, A., Vasiljevic, D., Viterbo, P., Woollen, J., 2005. The ERA-40 *Re*-analysis. Quart. J. Roy. Meteor. Soc. 131, 2961–3012.
Weaver, A.J., Sarachik, E.S., 1990. On the importance of vertical resolution in certain ocean general circulation models. J. Phys. Oceanogr. 20, 600–609.
Wunsch, C., Roemmich, D., 1985. Is the North Atlantic in sverdrup balance? J. Phys. Oceanogr. 15, 1876–1880.
Wunsch, C., 2011. The decadal mean ocean circulation and sverdrup balance. J. Mar. Res. 69, 417–434.
Xu, X., Chassignet, E.P., Price, J.F., Özgökmen, T.M., Peters, H., 2007. A regional modeling study of the entraining Mediterranean outflow. J. Geophys. Res. Oceans 112, C12005.
Xu, X., Schmitz Jr, W.J., Hurlburt, H.E., Hogan, P.J., Chassignet, E.P., 2010. Transport of Nordic seas overflow water into and within the Irminger sea: an eddy-resolving simulation and observations. J. Geophys. Res. Oceans 115, C12048.
Xu, X., Schmitz Jr., W.J., Hurlburt, H.E., Hogan, P.J., 2012. Mean Atlantic meridional overturning circulation across 26.5°N from eddy-resolving simulations compared to observations. J. Geophys. Res. Oceans 117, C03042.
Xu, X., Rhines, P.B., Chassignet, E.P., 2016. Temperature-salinity structure of the North Atlantic circulation and associated heat and freshwater transports. J. Clim. 29, 7723–7741.
Xu, X., Rhines, P.B., Chassignet, E.P., 2018. On mapping the diapycnal water mass transformation of the North Atlantic ocean. J. Phys. Oceanogr. 48, 2233–2258.
Xu, X., Chassignet, E.P., Wallcraft, A.J., Arbic, B.K., Buijsman, M.C., Solano, M., 2022. On the spatial variability of the mesoscale sea surface height wavenumber spectra in the Atlantic ocean. J. Geophys. Res.Oceans. 127, e2022JC018769.